

Contents lists available at ScienceDirect

# Colloids and Surfaces A: Physicochemical and Engineering Aspects

journal homepage: www.elsevier.com/locate/colsurfa



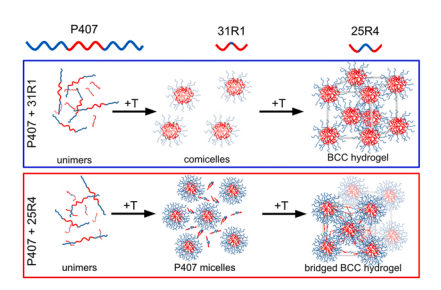


# Impact of small molecule and reverse poloxamer addition on the micellization and gelation mechanisms of poloxamer hydrogels

Joanna M. White a,1, Michelle A Calabrese a,\*,2

<sup>a</sup> University of Minnesota, 421 Washington Ave SE, Minneapolis, 55455 MN, USA

#### GRAPHICAL ABSTRACT



#### ARTICLE INFO

Keywords: Hydrogel Poloxamer Pluronic Self-assembly Drug delivery

#### ABSTRACT

Poloxamer 407 (P407) is widely used for targeted drug-delivery because it exhibits thermoresponsive gelation behavior near body temperature, stemming from a disorder-to-order transition. Hydrophobic small molecules can be encapsulated within P407; however, these additives often negatively impact the rheological properties and lower the gelation temperatures of the hydrogels, limiting their clinical utility. Here we investigate the impact of adding two BAB reverse poloxamers (RPs), 25R4 and 31R1, on the thermal transitions, rheological properties, and assembled structures of P407 both with and without incorporated small molecules. By employing a combination of differential scanning calorimetry (DSC), rheology, and small-angle x-ray scattering (SAXS), we determine distinct mechanisms for RP incorporation. While 25R4 addition promotes inter-micelle bridge formation, the highly hydrophobic 31R1 co-micellizes with P407. Small molecule addition lowers thermal transition temperatures and increases the micelle size, while RP addition mitigates the decreases in modulus traditionally associated with small molecule incorporation. This fundamental understanding yields new strategies for tuning the mechanical and structural properties of the hydrogels, enabling design of drug-loaded formulations with ideal thermal transitions for a range of clinical applications.

#### 1. Introduction

Poloxamers are amphiphilic ABA triblock copolymers composed of

hydrophilic poly(ethylene oxide) (PEO) endblocks and a hydrophobic poly(propylene oxide) (PPO) midblock, which are widely used as cosmetics [1], foaming agents [2–4], and emulsifiers [5–7]. Poloxamers

E-mail address: mcalab@umn.edu (M.A. Calabrese).

https://doi.org/10.1016/j.colsurfa.2021.128246

<sup>\*</sup> Corresponding author.

<sup>&</sup>lt;sup>1</sup> [orcid=0000-0002-5323-4332].

<sup>&</sup>lt;sup>2</sup> [orcid=0000-0003-4577-6999].

have also received considerable attention as drug delivery vehicles and pharmaceutical excipients due to their low toxicity, wide range of commercially-available formulations, and temperature-sensitive micellization behavior [8–19]. For example, the addition of poloxamers to aqueous drug solutions has been shown to improve bioavaliability and delivery efficiency, increasing residence time, accumulation, and transport across the blood-brain and intestinal barriers in comparison to free drug systems [20,21]. Accordingly, poloxamers have been approved by the FDA for oral, intravenous, topical, and intramuscular delivery, among others [19].

In aqueous poloxamer solutions, the temperature-dependent selfassembly behavior is driven by worsening interactions between the hydrophobic PPO midblock and water with increasing temperature, leading to the formation of spherical micelles near ambient conditions [21–26]. As aggregation of unimers into spherical micelles is associated with a slight decrease in viscosity [27,28], these liquids are ideal for handling and injecting for a range of applications. Additionally, micelle formation enables encapsulation of hydrophobic small molecules, like pharmaceuticals, that otherwise have poor solubility in water [12–18]. Further increasing the temperature in concentrated poloxamer formulations triggers the low-viscosity micellar liquids to order into physical soft hydrogels [14,21–25,29–32], making them of particular interest for topical, periodontal and ophthalmic drug-delivery routes [19,33,34]. Hydrogel formation occurs as the micelles undergo a disorder-to-order transition, forming a range of ordered phases including cubic-packed spheres and hexagonally-packed cylinders [21-25]. As the underlying structure of these materials dictates the rheological properties and applications, much work has been devoted to understanding and tuning these structural transitions.

Poloxamer 407 (P407) is one of the most widely used poloxamers in biomedicine, as gelation occurs near body temperature for modest polymer concentrations (15–30% w/w) [11,21,24,35–38]. Additionally, P407 is composed of 70% wt PEO, leading to high solubility and stability in aqueous solution. A number of studies have shown that P407 can encapsulate hydrophobic small molecules within the micelle core, enabling formation of drug-loaded formulations that flow at room temperature, allowing for ease of administration [12–18]. The resulting formulations gel near body temperature and have good adherence to biological tissues and membranes due to their soft moduli and high water content [14,29–32]. As a result, thermoresponsive poloxamer-based hydrogels have been widely studied and employed for non-invasive, extended, targeted delivery of drugs across biological barriers, such as the eye [33,39,40], skin [34,41], and eardrum [38,42–44].

Unfortunately, thermoresponsive drug-loaded gels composed purely of P407 often suffer in clinical applications due to low gelation temperatures and dynamic moduli [14-18,21,42,45]. For example, Yang and colleagues developed a drug-loaded P407 hydrogel for the treatment of otitis media (middle ear infections) [42]. This hydrogel was formulated to flow when injected into the ear canal and subsequently gel upon contacting the warmer tympanic membrane (TM, i.e. eardrum), enabling non-invasive delivery of the antibiotic Ciprofloxacin (Cipro) across the TM and directly into the middle ear [42-44]. In addition to Cipro, small molecule chemical permeation enhancers (CPEs) were incorporated to enhance diffusion across the tympanic membrane by disrupting the crystalline structure of the lipid bilayer [42,44,46]. As addition of these small molecules weakened the thermo-responsiveness and TM adhesion in P407 gels, Yang et al. chemically modified P407 by adding two hydrophobic polybutyl-phosphoester (PBP) end groups to form a pentablock copolymer that could reinforce the hydrogel via inter-micelle bridging [42]. While this P407-PBP copolymer was successful in eradicating otitis media in chinchillas [42], its toxicity and degradation products are unknown due to lack of clinical trial data, creating potential safety issues and regulatory hurdles.

To avoid the use of new chemistries with potential toxicities, the rheological properties of drug-loaded hydrogels can be enhanced by

addition of reverse poloxamers (RPs). Reverse poloxamers are BAB triblock polymers that contain the same block chemistries as poloxamers, but are arranged in the reverse order, with PPO endblocks and a PEO midblock. RPs have low toxicities, comparable to those of poloxamers [47,48], and they have the same chemical composition and degradation products. Further, RPs have been successfully used in *in vivo* animal trials and *in vitro* studies on lymph node cells without negative side effects [49].

While micelle formation in aqueous solutions is thermodynamically favorable for ABA poloxamers, BAB reverse poloxamers often do not assemble into micelles in water, as polymer chains must form loops to enable insertion of both PPO endblocks into the core [50]. As such, high PPO-fraction RPs like 31R1 do not form micelles in aqueous solutions at any temperature across a broad array of concentrations [51,52]. However, RPs with smaller PPO fractions like 25R4 can form flower-like micelles at high concentrations [53–55]. D'Errico and colleagues [53] constructed a morphology diagram for aqueous 25R4 as a function of temperature and concentration using small-angle x-ray and neutron scattering (SAXS/SANS). At ambient conditions and low concentrations (<5% w/w), 25R4 chains form Gaussian coils. With increasing concentrations and temperatures, the PPO blocks dehydrate and the chains organize into bridged micelles, with most PPO endblocks inserting into different micelle cores.

Reverse poloxamer addition can also significantly alter the selfassembly of traditional aqueous poloxamers [50,54,56-59]. While the formation of flower-like micelles requires an RP chain conformation that is entropically unfavorable, RPs have been hypothesized to form physical bridges between neighboring micelles composed of ABA poloxamers [50,56]. The impact of network connectivity on the mechanical and transport properties was recently examined in similar aqueous systems containing blends of AB diblock and ABA triblock polymers. Here, Rankin and colleagues found that increasing the fraction of triblock polymer promotes bridging, resulting in greater gel moduli [60]. Despite these enhanced mechanical properties, strengthened network connectivity due to bridging did not negatively affect small-molecule diffusion when compared at constant total polymer content [60]. Further, the addition of 25R4 has been shown to enhance gel stability and slows gel erosion in aqueous environments [61]. As such, thermoresponsive gels composed of bridged poloxamer micelle networks are promising candidates for targeted topical drug delivery.

To date, no studies have comprehensively investigated the impact of RP addition on the microstructure of P407 hydrogels using small-angle x-ray and neutron scattering techniques. Further, no works studied the effect of RP addition on the self-assembly and mechanical properties of poloxamer systems with incorporated small molecules. In this article, we use a combination of differential scanning calorimetry (DSC), linear viscoelastic shear rheology, and small-angle x-ray scattering (SAXS) to show that addition of 25R4 and 31R1 to P407 solutions in various molar ratios changes the micellization temperature, gel temperature, and mechanical properties of the gel, as well as micelle size and packing. Further, we demonstrate that these hydrogels can remain stable at physiological conditions upon addition of ciprofloxacin and chemical permeation enhancers. These P407-RP hydrogels thus represent an improvement over previous systems [42], as they are made entirely from chemistries with known biocompatibility and harmless degradation products, making them promising candidates for non-invasive drug delivery.

# 2. Materials and methods

#### 2.1. Materials

Kolliphor P407 was purchased from Sigma-Aldrich Corp. and reverse pluronics, 31R1 and 25R4, were obtained from BASF. The approximate molecular weights and block fractions of the triblock polymers are included in Table 1. The weight fractions of each block were confirmed

**Table 1** Approximate poloxamer molecular weights  $(M_n)$ , PPO block fraction  $(x_{PPO})$ , and PPO block molecular weight  $(M_{n,PPO})$  for P407 and relevant reverse poloxamers. PEO blocks are represented in blue and the PPO blocks are represented in red.

Polymer	$M_n$ [kDa]	X <sub>PPO</sub>	$M_{n,PPO}$ [kDa]	Formula	Structure
P407	12.6	0.3	3.8	EO <sub>100</sub> PO <sub>65</sub> EO <sub>100</sub>	VVVVV
25R4	3.8	0.6	2.3	PO <sub>20</sub> EO <sub>35</sub> PO <sub>20</sub>	
31R1	3.4	0.9	3.1	PO <sub>27</sub> EO <sub>8</sub> PO <sub>27</sub>	

using  $^1\text{H}$  NMR as detailed in SI.1. Sodium dodecyl sulfate ( $\geq$  99.0%), (R)-(+)-Limonene (97%), and ciprofloxacin ( $\geq$  98%) were purchased from Sigma-Aldrich Corp and bupivacaine hydrochloride (> 98.0%) was purchased from Tokyo Chemical Industry. All chemicals were used as received with no additional purification. Samples were formulated using distilled water.

#### 2.2. Sample preparation

P407 stock solutions (15% wt/v) were prepared using the well-established "cold method" [42,62–65], where the polymer was added to water and stirred at 4 °C for at least 24 hrs to yield a homogeneous and transparent solution. The aqueous solubility of ciprofloxacin is improved between pH 3-4 [66,67], so the pH of solutions with incorporated small molecules was adjusted to this range using  $\sim 50\text{-}100\,\mu\text{L}$  of 1M HCl. Ciprofloxacin (1% wt/v), bupivacaine (0.5% wt/v), sodium dodecyl sulfate (1% wt/v), and limonene (2% wt/v) were added to the stock solution and stirred at 4 °C for at least 24 hrs. These concentrations were selected as they were shown by Yang and colleagues [42] to successfully eradicate the bacteria associated with middle ear infections when contained within a P407-based gel. Following dissolution, reverse poloxamers (25R4 or 31R1) were added in molar ratios (P407:RP) of 1:0.5, 1:1, or 1:2. The solution was again stirred at 4 °C for  $\geq$ 24 h before use.

#### 2.3. Oscillatory rheology temperature ramps

The sol-gel transition was measured using oscillatory shear rheology on an Anton Paar MCR 302 stress-controlled rheometer with a 26.7 mm concentric cylinder double-gap geometry. Measurements were conducted near the linear viscoelastic (LVE) region ( $\gamma=1\%,\,\omega=1$  rad/s) with a gap of 1 mm and a temperature ramp rate of 1 °C/min. Representative amplitude sweeps to show the proximity to the LVE region at low and high temperatures are included in SI.3. The samples were held at 7.5 °C for 20 minutes prior to the temperature ramp to allow for temperature equilibrium to be reached and to erase any loading effects. The profile of G' versus temperature was fit to a sigmoidal function to extract values for the gelation temperature,  $T_{gel}$ , representative fits are in SI.4. The transition range, bounded by  $T_{low}$  and  $T_{high}$ , was defined as when the slope of the G' versus temperature plot was greater than 5 Pa/°C [68]. To assess reproducibility and statistical significance, all measurements were run in triplicate (see SI.19).

## 2.4. Differential scanning calorimetry (DSC)

Micellization temperatures were determined using Differential Scanning Calorimetry (DSC) on a TA Instruments Q1000 DSC. Samples were loaded in Tzero aluminum pans at 25  $^{\circ}\text{C}$  and quickly cooled to 7  $^{\circ}\text{C}$ . The pans were held at 7  $^{\circ}\text{C}$  to allow for the formulations to reach equilibrium before being heated at 1  $^{\circ}\text{C}/\text{min}$  to 50  $^{\circ}\text{C}$ . This ramp rate matches

that used for the rheology temperature ramps, allowing for the data obtained from the two ramps to be directly compared. The formation of micelles occurs over a broad range of temperatures [24,56,69,70]. The temperature at which the peak occurs in the heat flow curve is commonly reported as the micellization temperature,  $T_{mic}$ , as micelle formation reaches its maximum at this temperature [70,56]. The  $\Delta H_{mic}$ was determined by integrating the heat flow curve around the micellization peak using a linear baseline. The shape of the heat flow curve for formulations containing pure P407 or P407 with 31R1 can be well-described using an asymmetric double sigmoidal function where there is a small high-temperature tail commonly reported for P407 micellization (see SI.12) [24,56,69,70]. Addition of 25R4 results in the development of a high-temperature shoulder and, for high molar ratios, a secondary peak. In these cases, the  $\Delta H_{mic}$ , defined as only the area under the primary peak (without high-temperature secondary shoulder), was separated from the total area under the curve. To do so, the linear baseline was subtracted from the heat flow curves and the primary peak was again fit to a asymmetric double sigmoidal function. The area under this fitted curve was taken to be  $\Delta H_{mic}$ . This value was subtracted from the total area under the heat flow curve and the remainder was taken to be the area of the secondary peak,  $\Delta H_b$ . Further details on the fitting as well as representative fits are included in SI.12. This fitting procedure is similar to that performed by Ren and colleagues [71] for DSC curves with a similar shape.

#### 2.5. Small-angle x-ray scattering (SAXS)

#### 2.5.1. Experimental

Micelle size and packing was determined using small-angle x-ray scattering (SAXS). SAXS measurements on the formulations without small molecules were conducted at the University of Minnesota Characterization Facility on the Xenocs Ganesha instrument. The instrument uses an x-ray microsource with Cu target and integrated monochromator to generate x-rays with a wavelength of  $\lambda=1.54$  Å. Data were collected within a scattering vector range of 0.009 < q < 0.3 Å $^{-1}$  using an exposure time of 45 minutes. Calibration was performed using silver behenate, and 2D scattering patterns were azimuthally integrated using DataSqueeze [72] to generate 1D traces of scattering intensity, I(q) versus q. Samples were loaded into sandwich cells with Kapton covers, and temperature was controlled using a four-position INSTEC heating stage.

SAXS on small-molecule-containing samples was conducted on beamline 5-ID-D at the Advanced Photon Source of Argonne National Laboratory. A wavelength of  $\lambda=0.7293$  Å and sample-to-detector distance of 8.504 m were used to give a scattering vector range of  $0.002 < q < 0.192 ~\rm{\AA}^{-1}$ . Samples were loaded into aluminum DSC pans, and temperature was controlled using a Linkam stage to obtain scans every 5 °C between 5 °C and 50 °C. Five 1 s scans were performed at different positions around the pan, and each sample was loaded and measured in duplicate.

#### 2.5.2. Fitting

For temperatures between  $T_{mic}$  and  $T_{gel}$ , the poloxamers organize into disordered micelles and the one-dimensional SAXS intensities were fit to a spherical core-shell form factor with hard-sphere structure factor, as is typical for concentrated P407 micelles [28,73,74]. Prior to fitting, the background scan of the blank sample holder (sandwich cell or DSC pan) was subtracted. Five parameters were used to fit the data: average radius of the core  $(R_{core})$ , average radius of the shell  $(R_{shell})$ , electron density of the shell ( $\rho_{shell}$ ), polydispersity ratio (PDI), and volume fraction of hard spheres ( $\phi$ ). As  $\rho_{shell}$  and  $\rho_{core}$  are cross-correlated with  $R_{shell}$  and  $R_{core}$ , one of these parameters must be held constant to gain information about the relative size and composition of the core and shell. At this P407 concentration and temperature, the core is expect to be solvent-free [24, 75]. As such, for the systems containing pure P407 and P407 with RP, the electron density of the core is assumed to be that of pure PPO. For the structure factor, the radius of the hard spheres is assumed to be equal to that of the sum of the radii of the core and shell. This is a valid assumption for systems at high concentrations [76]. The electron density of the solvent was held constant and assumed to be that of pure water. Further information and representative fits are included in SI.5.

Above  $T_{gel}$  the poloxamer micelles often order into crystalline packings that result in the appearance of Bragg diffraction peaks. To determine the packing structure, the primary peak,  $q^*$ , was identified and then the ratios of subsequent peaks to  $q^*$  were evaluated. Face-centered cubic (FCC) packings were identified by peaks at  $q/q^*$  ratios of 1,  $\sqrt{4/3}$ ,  $\sqrt{8/3}$ ,  $\sqrt{11/3}$ , and  $\sqrt{12/3}$  which correspond to the (111), (200), (220), (311), and (222) planes, respectively and body-centered cubic (BCC) packings were identified by peaks at  $q/q^*$  of 1,  $\sqrt{2}$ ,  $\sqrt{3}$ ,  $\sqrt{4}$ , and  $\sqrt{5}$  corresponding to the (110), (200), (211), (220), (310) planes [77]. From the value of  $q^*$ , the lattice parameter of the cubic cell can be determined. The total micelle radius,  $R_b$  was approximated as half of the nearest neighbor distance,  $D_{nn}$ , between lattice sites.

#### 3. Results and discussion

#### 3.1. Bare P407 formulations

To develop a delivery system with clinically-applicable gelation temperatures, kinetics, and mechanical stability, the rheological and corresponding microstructural transitions of pure P407 in water (no small molecules or RPs) must be well understood, as micelle arrangement and size directly impact poloxamer mechanical properties, adhesion, and diffusion [64,78]. Here, the concentration of P407 was held constant at 15% (w/v). At lower concentrations (12% w/v), the number of micelles in solution is not large enough for significant inter-micelle interactions or overlap, so the micelles do not exhibit a substantial thermal response (SI.6). Conversely, at higher concentrations (18% w/v), the large number of micelles drives the formation of a densely-packed gel (SI.6), hindering small-molecule diffusion [42,60]. At 15% (w/v), the well-studied system of P407 in water [9,21,79-81] assembles into spherical micelles composed of PPO cores and PEO coronas with an average micellization temperature,  $T_{mic}$ , of 19.7  $\pm$  0.4 °C, defined as the temperature at which the endothermic peak in the DSC trace reaches its maximum value (Fig. 1a). Corresponding SAXS at 25 °C (Fig. 1b) exhibits two broad peaks, signifying the presence of disordered micelles in solution of total radius  $R_t = 98 \text{ Å}$  (see SI.7 for fit). As the temperature is further increased, the final chains in solution incorporate into micelles, and the DSC heat flow curve subsequently returns to the baseline value (Fig. 1a). Integrating the heat flow curve gives an enthalpy of micellization,  $\Delta H_{mic}$ , of 24.1  $\pm$  0.3 J/(g P407) in solution.

As the final chains are removed from solution and inserted into micelles, the micelles pack into a face-centered cubic (FCC) structure (Fig. 1b), consistent with other studies using unpurified P407 [82–84]. Mortensen and others [80,85] showed that presence of diblock impurities drives P407 systems to form FCC-packed micelles, and when the impurities are removed, the systems instead favor a BCC packing at the same polymer concentration. Size exclusion chromatography on the Kolliphor P407 used in this study has a low-molecule-weight shoulder,

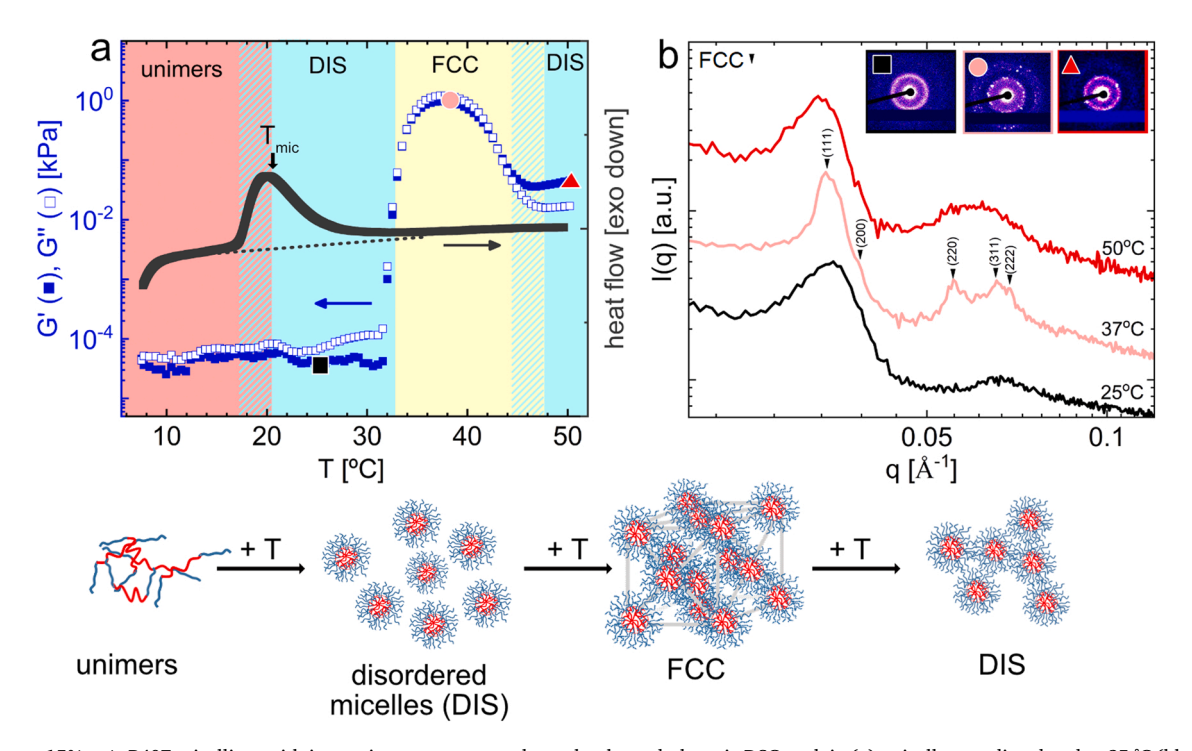


**Fig. 1.** Aqueous 15% w/v P407 micellizes with increasing temperature, shown by the endothermic DSC peak in (a); micelles are disordered at 25 °C (black trace, b). With further temperature elevation, a sharp increase in G' and G'' is observed (a) as the micelles pack into FCC structures, shown in (b) at 37 °C (pink). Above physiologically-relevant conditions, the moduli decrease (a) as the micelles disorder (b, red). (b, inset) Corresponding 2D SAXS patterns at 25, 37 and 50 °C. (For interpretation of the references to color in this figure legend, the reader is referred to the web version of this article.)

suggesting the presence of these impurities that drive FCC packings (see SI.2). The disorder-to-order transition from a low-viscosity liquid to a soft solid corresponds to a sharp increase in the storage and loss moduli, G' and G''. While gelation is often defined as the crossover of G' and G''[56,59,63,86], this criterion is dependent upon the frequency of the measurement [87]. Instead, in this work, the onset of gelation  $T_{low}$  is defined as the point where the slope of the G' vs. T exceeds 5 Pa/°C. Here,  $T_{low}$  occurs at 31  $\pm$  1 °C and the maximum storage modulus,  $G'_{max}$ , is achieved at 37  $\pm$  1 °C (Fig. 1a). The temperature-dependent storage modulus over the course of this transition is well described by a sigmoid, the center of which,  $T_{geb}$  occurs at 34  $\pm$  1 °C (see SI.4). Corresponding SAXS patterns confirm this disordered micelle-to-FCC transition (Fig. 1b, inset), where the lattice parameter,  $a_{FCC}$ , of 318 Å at 37 °C suggests a micelle radius of  $R_t = 112$  Å; here,  $R_t$  is approximated as one-half of the nearest neighbor distance,  $D_{nn}$ . Unsurprisingly, this radius is larger than that for disordered micelles at 25 °C, due to both the greater number of P407 chains per micelle,  $N_{agg}$ , incorporated at higher temperatures and thermal expansion [28]. As temperature is increased beyond physiological conditions, the moduli plateau and then begin decreasing substantially near 40 °C (Fig. 1a). The absence of an exothermic peak in the DSC traces suggests that this reduction in moduli is not due to de-micellization, but rather to an order-to-disorder transition (ODT). This ODT is confirmed by a disappearance of the FCC peaks in the SAXS patterns at 50 °C (Fig. 1b) and is consistent with prior work on P407 [63,86,88]. Suman and colleagues [86] attribute this ODT to dehydration of the PEO blocks in the corona, where the decreasing PEO solubility with increasing temperature causes the micelle coronas to aggregate, pulling the micelles out of the lattice structure.

#### 3.2. Effect of reverse poloxamer addition on micellization

Despite similar overall molecular weights, adding 25R4 versus 31R1 to the bare P407 systems drastically impacts the self-assembly behavior, thermal transitions, and rheological properties; see SI.11 for statistical analyses of these parameters. For both 25R4 and 31R1 at molar ratios of 1:0.5, 1:1, and 1:2 mol P407:mol RP, increasing RP molar ratio is linearly correlated with a reduction in  $T_{mic}$ , shown by the decreasing peak locations in the DSC traces (Fig. 2a,b). As the critical micelle

temperature (CMT) decreases with increasing poloxamer content [26, 83,84], this reduction in  $T_{mic}$  with added RP is in part due to the increase in total polymer concentration from 13% wt in bare P407 to  $\sim$  19% wt for 1:2 P407:RP. Despite the fact that 31R1 contains a higher fraction of hydrophobic PPO, adding 25R4 reduces  $T_{mic}$  more substantially than adding an equivalent amount of 31R1 (Fig. S.12), with a temperature-reducing strength of 3.7  $\pm$  0.4 °C/(g 25R4) vs. 2.3  $\pm$  0.6 °C/(g 31R1). Consistent with prior work [57,70] this trend can be explained by differences in the "effective" P407 concentration. Here, the added RP PEO-blocks associate with water molecules, reducing the available water content around P407 and effectively increasing its concentration. Water association is more significant in solutions containing 25R4, which is 40% PEO by weight; conversely, 31R1 is only 10% wt PEO, so the effective concentration of P407 increases less with 31R1 addition.

The distinct block ratios of the two RPs also leads to markedly different micellization mechanisms, reflected by the trends in the enthalpy of micellization with added RP (Fig. 2a–c); here  $\Delta H_{mic}$  is determined as the area under the primary peak in the DSC trace. Per gram of total polymer,  $\Delta H_{mic}$  increases steeply with increasing 31R1 content but decreases with 25R4 content; see SI.11 for comparisons of  $\Delta H_{mic}$  on additional bases (J/(g P407), J/(g PPO)). Interestingly, 25R4 addition results in the development of a high-temperature shoulder or broad secondary peak in the heat flow curve denoted as  $\Delta H_b$  (Figs. 2a, SI.12), reminiscent of prior work on P407/25R4 solutions [57,70].

Thermal ordering transitions in P407/25R4 solutions are hypothesized to occur via a process with two distinct steps (Fig. 5), where bridging ( $\Delta H_b$ ) follows P407 micellization ( $\Delta H_{mic}$ ). In step one, PPOwater interactions become less favorable with increasing temperature, driving the P407 chains to form micelles. Note that poloxamer micellization is driven almost entirely by the PPO block [26,89], and that micellization of P407 is expected at lower temperatures than for 25R4 because its PPO molecular weight is over three-fold larger than that of a 25R4 PPO endblock [70]. Additionally, the RP chain conformation required to form flower-type micelles with both PPO blocks inserted into the core is entropically unfavorable [55–57], thus micelles are often not observed at low 25R4 contents [53]. This proposed first step is consistent with prior work suggesting that the primary DSC peak in

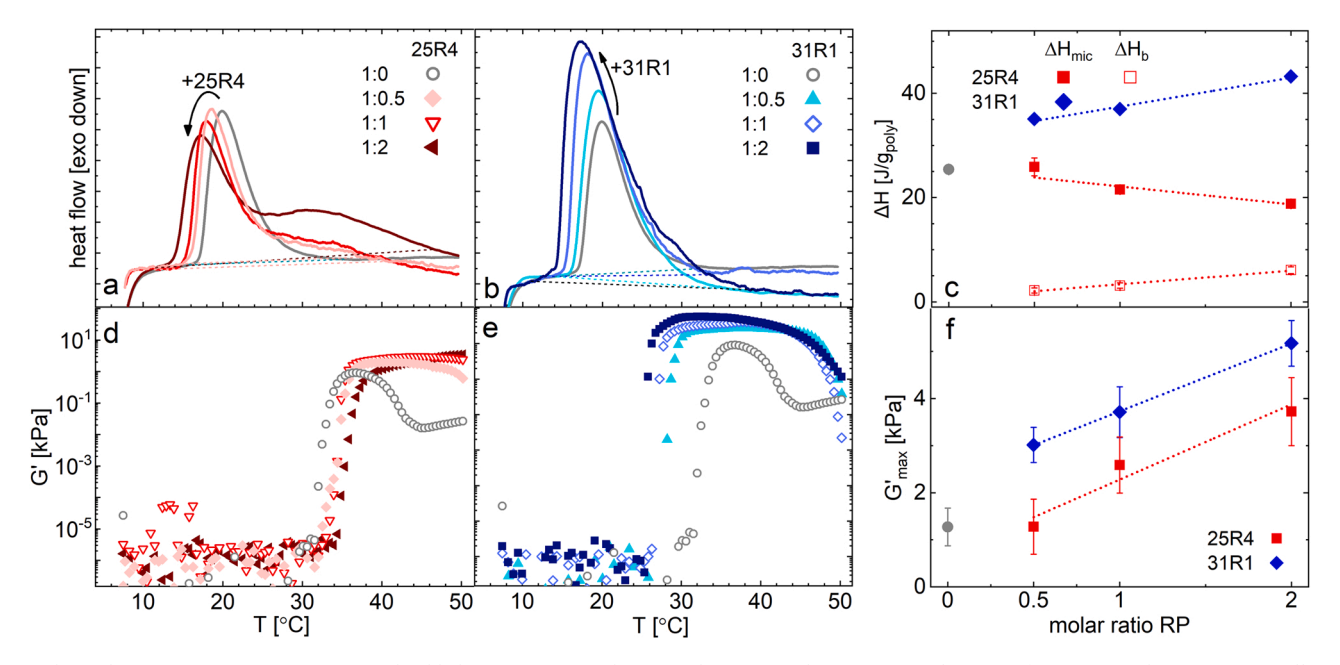


**Fig. 2.** Thermal transitions in 15% w/v P407 with added 25R4 or 31R1, where  $T_{mic}$  decreases with increasing molar ratio of (a) 25R4 or (b) 31R1. (c) Micellization enthalpies,  $\Delta H_{mic}$  [J/g polymer], strongly depend on RP identity. With increasing 25R4 content,  $\Delta H_{mic}$  decreases and a high-temperature secondary peak appears, attributed to bridging  $\Delta H_{b}$ . Conversely,  $\Delta H_{mic}$  increases with increasing 31R1 molar ratio. (d,e) Linear viscoelastic rheology indicates that the onset of gelation increases with 25R4, but decreases with 31R1, addition. (f) In formulations containing RP,  $G'_{max}$  increases linearly with RP content.

P407/25R4 solutions is largely due to P407 micellization [57,70] When the temperature is further increased (step two), interactions between water and the 25R4 PPO endblocks worsen, making 25R4 bridging potentially favorable [53,57,70]. We thus suspect that the secondary shoulder in the DSC trace corresponds to the caloric penalty for de-solvating the 25R4 PPO blocks via bridging, to be discussed further in Section 3.3.

Evidence from SAXS and DSC also suggests that 25R4-containing solutions undergo a similar first step, primarily involving P407. The micelle core radii, Rc, for bare P407 and 25R4-containing solutions are similar in value at 20 °C, indicating a similar P407 aggregation number,  $N_{agg}$  (Table S3). Additionally, the rapid decline in  $\Delta H_{mic}$  with increasing 25R4 (J/(g polymer), Fig. 2c) is likely somewhat artificial due to the inclusion of 25R4 chains in the mass basis that do not participate in the micellization process. When  $\Delta H_{mic}$  is instead considered based on the PPO content in P407 (J/(PPO<sub>P407</sub>)),  $\Delta H_{mic}$  is similar in magnitude to that obtained for bare P407, where micellization is driven by desolvation of the P407 PPO groups (SI.11). Further, the enthalpy of micellization (J/ (PPO<sub>P407</sub>)) is uncorrelated with 25R4 content, supporting the hypothesis that 25R4 does not participate in the initial micellization phase. The full width at half maximum (FWHM) of the  $\Delta H_{mic}$  peak is also constant across formulations (Fig. S13), whereas co-micellization would likely broaden this transition.

Conversely, 31R1 is directly involved in the P407 micellization process, as evidenced by the single, broad endothermic peak in the DSC trace that increases in area with increasing 31R1 content (Figs. 2b,c). Unlike in 25R4-containing solutions, here the FWHM of the  $\Delta H_{mic}$  peak substantially widens (SI.11) and the micelle radius at 20 °C monotonically increases with 31R1 content (Table 2), suggesting that 31R1 co-micellizes with P407. The sharp increase in  $\Delta H_{mic}$  (J/(g polymer)) with increasing 31R1 content supports the co-micellization hypothesis (Figs. 2c, S15), as there are more PPO groups requiring desolvation per gram of polymer, because 31R1 has a larger PPO fraction than P407. However, when examined per gram total PPO (Fig. S17),  $\Delta H_{mic}$  is uncorrelated with 31R1-content (Fig. S15), and  $\Delta H_{mic}$  (J/(g PPO $_{total}$ )) is comparable to that for bare P407 and for 25R4-containing solutions (J/(g PPO $_{P407}$ )), further suggesting that 31R1 co-micellizes while 25R4 does not.

The difference in micellization mechanism can be explained by the sizes of each of the RP blocks (Table 1). While 25R4 has a PEO midblock of 1.5 kDa, the PEO block in 31R1 is only 0.3 kDa. Although the overall chain lengths are similar, the short PEO block in 31R1 is not long enough to span the PEO-rich coronas of P407 micelles as is necessary for bridging; bridging in 31R1 would thus unfavorably expose a large fraction of PPO endblocks to water. We instead propose that during comicellization, 31R1 incorporation into the core both increases the micelle size  $R_t$  and volume fraction  $\phi$  (Tables 2, S3) and "displaces" a number of P407 chains that can form additional micelles (Fig. 3). Consistent with recent modeling efforts on 31R1 [90], the 31R1 chains likely preferentially locate in the outer regions of the core due to the short PEO block (Fig. 3). Calculations based on the 31R1 and P407 chain

**Table 2** Morphology and micelle radius,  $R_b$  at 20 °C and 37 °C for various RP molar ratios. Average standard deviation for transition temperatures is  $\sim 0.6$  °C; see SI.19 for all values.

RP	Molar	$R_t$ [Å]	$T_{mic}$ [°C]	$T_{low}$ [°C]	$T_{gel}$ [°C]	Structure	$R_t$ [Å]
	ratio	20 °C				37 °C	37 °C
-	0	90.6	19.7	31.4	33.9	FCC	112.0
25R4	0.5	92.5	19.0	34.6	37.5	BCC	97.0
25R4	1	94.2	18.4	34.7	37.7	BCC	98.0
25R4	2	94.1	16.9	34.7	39.2	BCC	94.1
31R1	0.5	96.4	19.2	28.0	30.4	FCC	112.6
31R1	1	98.8	18.8	27.3	29.5	BCC	108.5
31R1	2	99.4	18.1	25.8	27.9	BCC	107.0

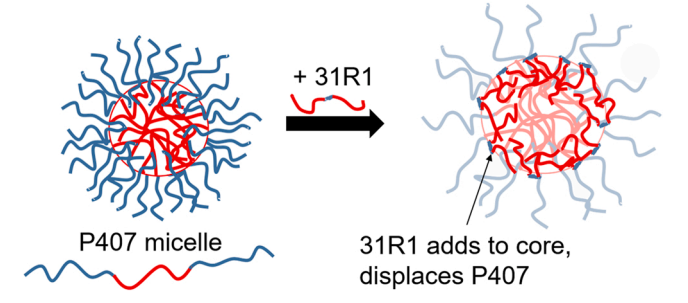


**Fig. 3.** Proposed mechanism of 31R1 co-micellization with P407, where 31R1 incorporates into the outer regions of the core. At high 31R1 content, 31R1 displaces several P407 chains, reducing the corona density and increasing core size.

volume, fits to SAXS data, and known component electron densities suggest that at the lowest 31R1 content (1:0.5 P407:31R1), the increase in  $R_t$  vs. bare P407 can be entirely attributed to 31R1 addition; no additional micelles are created (see SI.9, SI.10 for detailed calculations). However, in solutions of 1:1 and 1:2 P407:31R1, the total number of micelles increases by roughly 5% and 13%, respectively, decreasing the P407  $N_{\rm agg}$  by the same proportion. Accordingly, compared to bare P407, between two and three P407 chains per micelle are displaced in the 1:1 formulation, and between five and six P407 chains are displaced per micelle in the 1:2 formulation (SI.9, SI.10). Displacement of P407 chains by 31R1 is also expected to decrease the micelle corona density as fewer PEO chains from P407 decorate the corona (Fig. 3), likely having consequences for the subsequent gelation behavior and ordered phase formation.

## 3.3. Structure and gelation with reverse poloxamers

The proposed differences in micellization mechanism between solutions containing 25R4 versus 31R1 lead to opposite trends in rheological behavior observed during thermal gelation (Fig. 2d,e). While the maximum storage modulus,  $G'_{max}$ , increases with addition of either RP (Fig. 2f), the gelation temperature  $T_{gel}$  increases with 25R4 addition but decreases with 31R1 addition (Fig. 2d,e). The decreasing  $T_{gel}$  is consistent with the increasing volume fraction of micelles with 31R1 addition at 20 °C (Table S3), whereas  $\phi$  is nearly independent of 25R4 content at 20 °C. Interestingly, the onset of gelation,  $T_{low}$ , also decreases monotonically with 31R1 content, whereas  $T_{low}$  is independent of 25R4 content and is uncorrelated with  $T_{gel}$  (SI.11). Similar to bare P407, the moduli for both systems containing RPs decrease above physiological conditions; however, the reduction in modulus with temperature is substantially more severe in 31R1 solutions (Figs. 2d-e). This decrease in G' in 25R4 solutions is attributed to micelle rearrangement because samples remain optically clear and no exothermic peak is observed in the DSC traces (Figs. 2d, SI.13). However, in 31R1, a small endothermic feature appears in the DSC traces just below 40 °C, particularly evident in the 1:1 and 1:2 formulations (Fig. 2e). In poloxamers, this feature corresponds to macrophase separation at the cloud point [91], where the associated enthalpy is substantially lower than in the micellization transition because clouding is largely related to PEO, rather than PPO, solubility. Visual observations confirm that this drastic reduction in G' in 31R1 solutions corresponds to clouding (SI.13).

Rheology and SAXS measurements during gelation support the proposed mechanism of 31R1 adding to the micelle core. Bare P407 exhibits the highest  $T_{gel}$  ( $\sim$  34 °C, Table 2) and lowest  $G_{max}$  (Fig. 2e,f). Adding 0.5 mol 31R1 per mol P407 does not impact  $T_{mic}$  but doubles  $G_{max}$  and lowers  $T_{gel}$  by 3.5 °C, which is unsurprising based on the larger micelle size and volume fraction in the 1:0.5 formulation prior to gelation (Table 2). Gelation occurs when inter-micelle interactions and corona overlap enable a percolated network to form; forming the same number

of micelles but of larger size in the 1:0.5 formulation would thus shift the percolation threshold to lower temperatures in comparison to the pure P407 system. Consistent with both a larger micelle size and a larger number of micelles,  $T_{gel}$  further decreases at higher 31R1 content, where  $T_{gel}$  in the 1:2 formulation is  $\sim$  6 °C lower than in bare P407.

Despite the larger micelle size and volume fraction at ambient conditions in the 1:0.5 formulation, the micelles organize into an FCC packing similar to that formed in bare P407 (Fig. 4); the micelle radius in the gel is only slightly larger than that for the bare system at 37 °C (Table 2). As the 31R1 mass fraction is small compared to that of P407 (1.7% vs. 12.8% wt) and the P407  $N_{agg}$  is the same as in bare P407 (SI.9, SI.10), this small amount of 31R1 does not significantly change the packing. However, higher 31R1 molar ratios do impact packing, instead causing micelles to organize into a BCC morphology (Fig. 4). BCC formation is favored over FCC in systems with less-dense coronas [64,80, 92-94], and has been observed in P407 when co-micellized with other poloxamers or pure PPO [95,96]. This behavior thus further supports the proposed 'displacement' mechanism and corresponding calculations, as the corona density is reduced because fewer P407 PEO chains decorate the core (Fig. 3). Despite the relatively minor decrease in P407 aggregation number with 31R1 addition (between 2 and 6 P407 chains/micelle), the associated reduction in corona density appears significant enough to facilitate BCC formation in the 1:1 and 1:2 formulations. Notably, the micelle  $R_t$  values in these two formulations are within 5% of the bare P407 value at 37 °C (Table 2).

The proposed bridging mechanism in 25R4-containing solutions during gelation is also supported by rheology, DSC, and SAXS, where G'continually increases across temperatures spanning the endothermic shoulder in the DSC traces (Fig. 5). Interestingly, while  $G'_{max}$  increases monotonically when 31R1 is added, at the lowest 25R4 ratio (1:0.5 P407:25R4),  $G'_{max}$  is identical to that for the bare system (Fig. 2f). Despite the fact that at 20 °C, these solutions have similar micellization transition widths, volume fractions, core radii and total radii (Tables 2 and S3, Fig. S13), the gelation temperature increases with increasing 25R4 molar ratio. Micelles formed in solutions of 1:0.5 and 1:1 P407: 25R4 have statistically identical  $T_{gel}$  values, which are 2 °C higher than in bare P407; formulations at 1:2 P407: 25R4 transition 5 °C higher than the bare system (Table 2). If 25R4 chains co-micellized at this stage, either more micelles or much larger micelles would form; in this event, a reduction rather than increase in  $T_{gel}$  would be expected with increasing 25R4 content. The increasing  $T_{gel}$  with 25R4 content instead suggests that gelation is disrupted by 25R4. Mortensen et al. showed that the P407 disorder-to-order transition occurs at higher temperatures in the presence of diblock impurities [80], noting that if the impurities are not incorporated into micelles, these chains must occupy "empty" spaces between micelles [80]. If 25R4 acts similarly, the micelle overlap required for gelation would be impeded with increasing 25R4 content,

thereby raising  $T_{gel}$  until most 25R4 chains can sufficiently rearrange and bridge. Interestingly, the onset of gelation,  $T_{low}$ , is identical across 25R4-containing solutions (Table 2), consistent with the similar micelle size and volume fraction prior to gelation. However, adding 25R4 significantly broadens the gel transition from  $\sim 5$  °C (bare P407, 1:0.5 formulation) to over 15 °C in 1:2 P407:25R4 (Table S9), supporting the hypothesis that 25R4 disrupts corona overlap and long-range interactions.

The hypothesis of gelation disruption by 25R4 is supported by prior work and trends in  $G'_{max}$  and  $\Delta H_b$  with increasing 25R4 content. D'Errico et al. found that 25R4 could bridge by insertion into distinct micelle cores over length scales of 25–40 Å [53]. As the distance between two P407 cores is much larger than this length scale, 25R4 chains could span two micelle coronas via 'partial insertion,' where PPO is shielded from solvent by its proximity to dense corona regions. Alternatively, 25R4 could incorporate with one PPO block left dangling outside of the micelles [56,70]. To reduce the unfavorable PPO-water interactions, dangling PPO blocks could associate with one another, causing a physical bridging network across micelles that increases G' [56,57]. For all three formulations, the caloric penalty per gram PPO is less than half of that for the primary micellization transition (Fig. S16), which is unsurprising given that neither bridging mechanism results in complete desolvation of the 25R4 PPO groups.

At 37 °C, the 25R4-containing gels organize into BCC-packed micelles in contrast to the FCC packing found in bare P407 (Fig. 4); however, notably, these solutions appear to transition to an FCC configuration at even higher temperatures (SI.15). These BCC packings exhibit a dramatically lower lattice parameter and thus larger-thanexpected micelle number density when compared to bare P407 or their own FCC packings at even higher temperatures, suggesting that the BCC ordered phase does not span the entire hydrogel (Table 2). As noted by Mortensen and others [80,85], diblock impurities present in commercial triblocks may not always incorporate into the micelle, but instead may increase the lattice spacing and promote FCC formation via core densification. While ultimately FCC is achieved in 25R4-containing systems at high temperatures, initially, the diblock impurities and 25R4 might preferentially aggregate in disordered regions [97] that coexist with the ordered BCC phase. In this event, P407 micelles may form ordered domains of BCC-packed micelles, as is expected for low dispersity P407 [80,85], prior to the formation of a single ordered domain where impurities and bridging force FCC formation. The ability of 25R4 to reduce the dispersity of micelle sizes by association with impurities in solution is supported by SAXS measurements at 20 °C, where the polydispersity decreases continuously with increasing 25R4 content. The formation of coexisting disordered and ordered phases at 37 °C is also supported by the smearing (1:1) and disappearance (1:2) of the primary BCC peak upon 25R4 addition, suggesting a heterogeneous packing

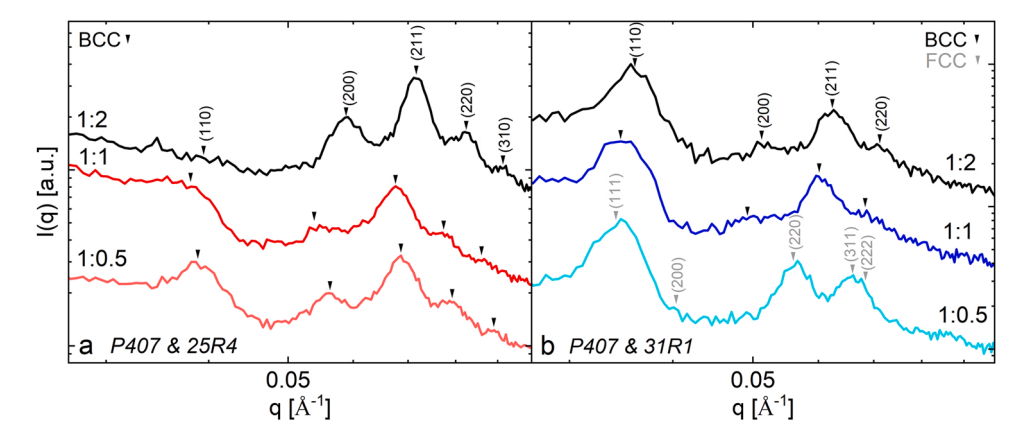


Fig. 4. 1D SAXS intensities at 37° C for formulations containing 25R4 (a) and 31R1 (b). Micelles pack into BCC ordered phases in all cases except at 1:0.5 31R1 where FCC-packing is observed.

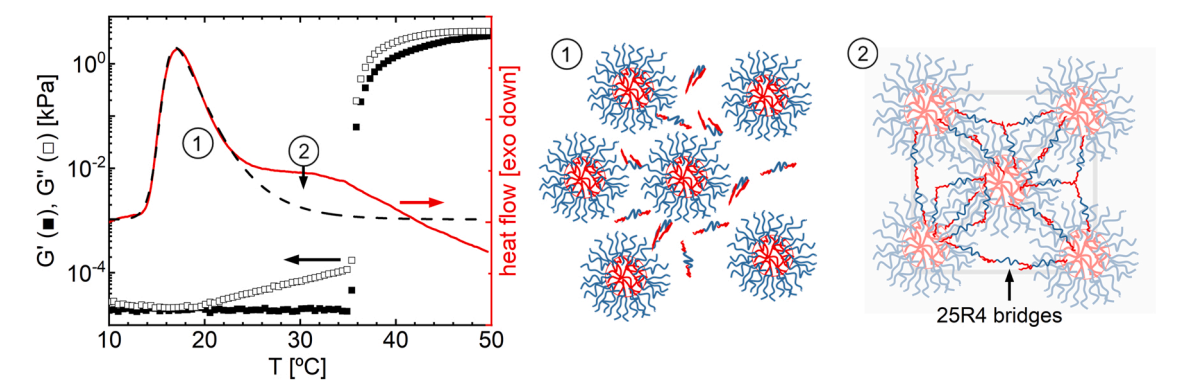


Fig. 5. DSC heat flow curve of 1:2 P407: 25R4 show a primary endothermic peak that corresponds to P407 micellization (fit in dashed lines, see SI.12), and a secondary shoulder for 25R4 incorporation. The 25R4 PPO blocks can either associate with one another or partially span two micelles, forming inter-micelle bridges that lead to a sharp increase in G' and G''.

structure. Further,  $T_{gel}$  is higher than 37 °C for all 25R4-containing solutions, and at temperatures above 37 °C, the impact of the molar ratio of 25R4 on the micelle packing supports the proposed two-step incorporation process. At the highest molar ratio of 25R4 (1:2), the formulations remain in a BCC packing up to 50 °C (SI.15). In this formulation, the dynamic moduli peak above 50 °C (particularly evident on a linear scale in Fig. S27), suggesting that a significant number of 25R4 chains have not yet formed bridges and remain in solution. In contrast, the systems containing lower molar ratios of 25R4 exhibit a BCC-to-FCC transition that aligns with the temperature of  $G'_{max}$  (SI.15). As discussed previously, 25R4 association across micelles contributes to the enhanced mechanical properties of 25R4-containing formulations in comparison to those with pure P407. As more 25R4 chains incorporate into the micelles, the density of the corona is expected to increase, driving FCC formation.

#### 3.4. Small-molecule incorporation

The addition of ciprofloxacin and CPEs to bare P407 shifts the micellization and gelation transitions to lower temperatures and significantly reduces the dynamic moduli of the resulting hydrogel (Fig. 6a). Small-molecule addition drastically increases the FCC lattice parameter (Fig. 6b), confirming that the hydrophobic small molecules incorporate into the micelle core, as expected [21,73,81,88]. The approximate micelle radius at 37 °C is 144 Å compared to 112 Å in pure

P407 (Table 3). Bupivacaine hydrochloride [98], limonene [99,100], and ciprofloxacin [101,102] are all sparingly soluble in water, making encapsulation in the core favorable. As a result, the core expands; without a significant increase in  $N_{\rm agg}$  to serve as reinforcement, the corona will become less dense and the micelle will be less structurally stable due to its expanded size, reducing the mechanical integrity of the gel.

As expected, the presence and type of RP impacts the structure and gelation mechanism in formulations containing small molecules. The effects of each RP on the small-molecule-loaded systems are explained using the high molar ratios of RP (1:2), where the structural transitions associated with micellization and gelation are shown via SAXS in Fig. 7b for 1:2 25R4:P407 with CPEs/Cipro. At low temperatures, there are no defined features in 1D SAXS intensity (Fig. 7b), indicating unimers in solution. Above the  $T_{mic}$  (Fig. 7a), the pattern exhibits two broad peaks which are well described by a core-shell spherical form factor for disordered micelles. As in the 25R4-containing formulations without small molecules, the onset of gelation,  $T_{low}$ , is independent of RP content; a pronounced secondary peak in the DSC trace spans the entire gelation transition (Fig. 7a). Following the onset of gelation, sharp Bragg peaks appear, signifying micelle ordering into an FCC-packed structure. As temperature increases further, the concentration of RP is high enough in the 1:2 formulation that the FCC crystalline packing is disrupted, further supporting the proposed bridging mechanism upon addition of

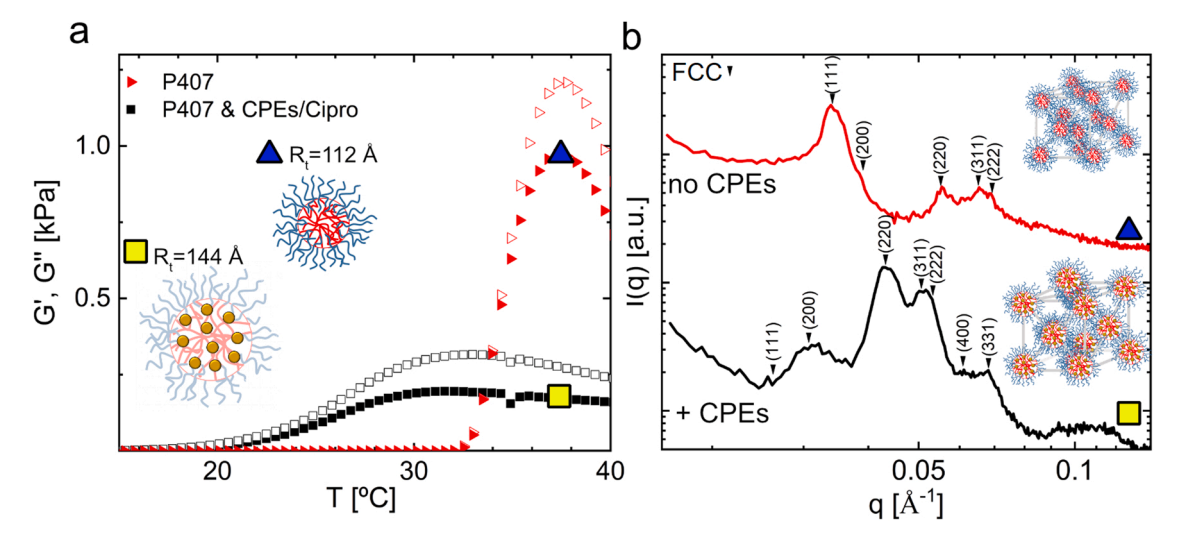


**Fig. 6.** (a) Adding small molecule CPEs and Cipro to aqueous P407 reduces the gelation temperature and resulting mechanical properties, G' (closed symbols) and G'' (open symbols). (b) At 37 °C, the lattice parameter for FCC phase is substantially larger for formulations containing small molecules, indicating an increase in the micelle size. Note that while adding small molecules often extinguishes the primary peak [88,103,104] (see Figs. 7, 8), FCC indexing for P407 with CPEs gives the expected  $R_t$  value (SI.18).

Table 3 Morphology, thermal transitions, and  $R_t$  at 37 °C for various RP molar ratios. Transition temperatures are for CPE-containing formulations. Average standard deviation for transition temperatures is 0.6 °C; see SI.19 for all values.

RP	Molar ratio	Structure bare	$R_t$ [Å] bare	Structure +CPEs	$R_t$ [Å] +CPEs	$T_{mic}$ [°C] +CPEs	$T_{low}$ [°C] +CPEs	$T_{gel}$ [°C] +CPEs
N/A	0	FCC	112	FCC	144	27.7	23.3	31.9
25R4	0.5	BCC	97	FCC	150	35.6	24.9	40.8
25R4	1	BCC	98	FCC	148	36.0	26.9	42.7
25R4	2	BCC	94	FCC	118	33.2	26.6	39.8
31R1	0.5	FCC	113	FCC	144	29.9	22.5	37.0
31R1	1	BCC	109	FCC	122	27.0	19.7	33.0
31R1	2	BCC	107	BCC	120	23.8	16.6	28.4

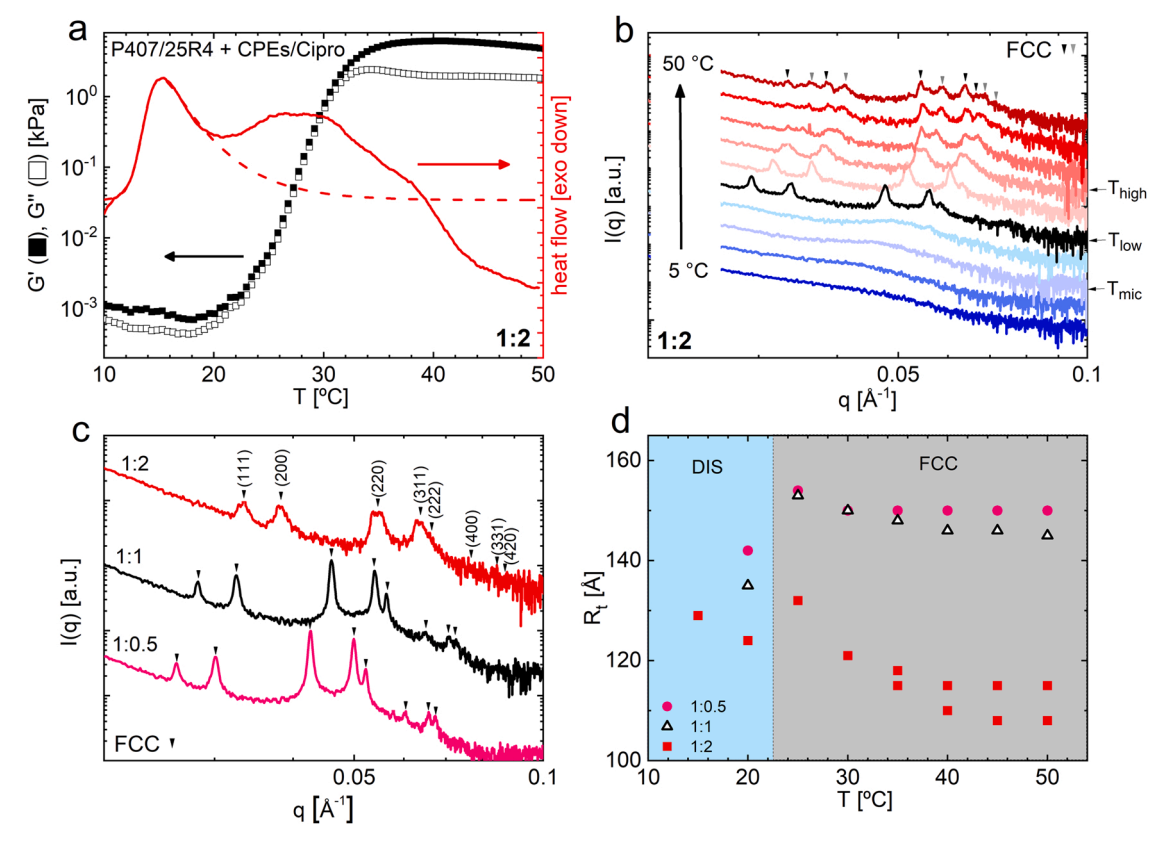


**Fig. 7.** (a) G'(T) (filled) and G''(T) (open) for 1:2 P407:25R4 with drug/CPEs. DSC thermographs (red) show a micellization peak prior to gelation. (b) SAXS intensities every 5 °C from 5 to 50 °C show a transition from unimers to disordered micelles to FCC-packed micelles with increasing T. At higher temperatures, FCC peaks smear and split, suggesting inter-micelle bridging. (c) The addition of 25R4 in increasing molar ratios causes a reduction in the FCC lattice parameter. (d) Micelle radii  $R_t$  were estimated as half of the nearest neighbor distance (ordered phases) and using a core-shell fit (disordered micelles).

25R4. This bridging behavior manifests as a smearing and eventual splitting of the crystalline peaks, such that two distinct FCC phases are formed (Fig. 7b,c). Despite reduction in crystalline order, this sample forms a more mechanically robust gel than the formulations with lower 25R4 content (Fig. 9d), attributed to strong inter-micelle bridging by RPs that can distort the P407 micelles from a perfect FCC packing [56, 70,103].

In contrast to pure P407 systems that exhibit a slight increase in lattice parameter with temperature due to thermal expansion [80], the FCC lattice parameter in the 1:2 formulation decreases significantly (~20%) with increasing temperature (Fig. 7d). This unexpected effect of temperature on the lattice parameter is also in contrast to the behavior of the 25R4-containing formulations without small molecules, where an increasing lattice parameter and modulus were observed with increasing temperature during the gelation process (SI.15). Here, a decrease in lattice parameter with increasing temperature implies a higher number density of micelles incorporated into the bridged network. As additives

like small molecules or RPs can impact the preferred P407 aggregation number, a number of additional micelles likely incorporate into the ordered structure with increasing temperature in the 1:2 P407:25R4 formulation with CPEs, pushing the micelles closer together and causing the formation of a stronger gel network.

Formulations containing smaller molar ratios of 25R4 (1:0.5 and 1:1) also form FCC packings upon heating; the formation of FCC rather than BCC structures across 25R4 formulations with small molecules is likely due to the largely expanded core size and increased core/corona ratio resulting from CPE encapsulation [64,80,92–95]. Unlike in the 25R4-containing solutions without small molecules, here the micelles are comparable in size to (or even slightly larger than) drug-loaded systems containing only P407. Further, the FCC crystalline peaks remain sharp and defined across the temperature range (Fig. S33). As in the 1:2 formulation, the micelle size at these two RP concentrations also decreases with increasing temperature during gelation (Fig. 7c–d). However, the extent of this reduction is lessened at lower molar ratios of

25R4. This trend suggests that the micelle aggregation number decreases with increasing RP content in favor of creating more micelles, which is unsurprising given that the micelle total radius prior to gelation (20 °C) also scales linearly and inversely with RP content (Figs. 7d, SI.17). Interestingly, the width of the gelation transition and  $T_{gel}$  are statistically identical for the 1:0.5 and 1:1 formulations, but both values decrease for the 1:2 formulation (SI.17). Thus, while  $T_{low}$  is identical across formulations, the large increase in number of micelles in the 1:2 formulation pushes gelation to lower temperatures and narrows the transition, in contrast to the behavior with increasing 25R4 content without CPEs present. For all three solutions containing 25R4 with small molecules, the decrease in micelle size and lattice spacing with increasing temperature plateaus above 40 °C. These plateaus correspond with both the temperature at which  $G'_{max}$  occurs (SI.17) and the temperature at which the final 25R4 chains are incorporated into the network (end of second DSC peak, Fig. 7a). The alignment between the DSC traces,  $G'_{max}$ , and the plateau in  $R_t$  further supports the hypothesis that the network is strengthened both by addition of new micelles and incorporation of 25R4 bridging strands.

Adding 31R1 has a dramatically different effect than adding 25R4 in small-molecule-loaded formulations. At low molar ratios of 31R1 (1:0.5), the micelles arrange into a defined FCC packing with a similar lattice parameter to the pure P407 system with CPEs. As observed in the systems without small molecules, here the low amount of RP does not significantly affect the packing (Fig. 8c). Once again, 1:2 P407:31R1 (with small molecules) is used to explain the behavior with added 31R1 (Fig. 8). Here, the micellization peak seen via DSC is even broader than that observed in the 31R1-containing solutions without small molecules, with an FWHM nearly twice as large (Figs. 8a, SI.16). Increasing molar ratios of 31R1 correlate with peak broadening and thus increasing  $\Delta H_{mic}$ . At temperatures near  $T_{mic}$ , the micelles organize into an FCC-

packed crystalline structure, as is the case for drug-loaded P407 systems without RP. Interestingly, this phase is not stable and the micelles quickly undergo an FCC-to-BCC transition as temperature is further increased (Fig. 8b). This transition is reflected in both the tail of the peak seen via DSC and the sharp increase in G' and G'' (Fig. 8a). Despite the fact that small-molecule incorporation increases the core size, this favored BCC packing is consistent with the mechanism proposed in the systems without small molecules, where 31R1 displaces a small number of P407 chains in the micelle core. Notably, the two formulations with lower 31R1 content (1:0.5 and 1:1) instead favor FCC formation due to the increased core/corona ratio (Fig. 8d). In contrast to drug-loaded 25R4 solutions, the 1:2 P407:31R1 formulations exhibit an increase in lattice parameter with increasing temperature (Fig. 8d), consistent with trends exhibited by overlapping poloxamer micelles undergoing thermal expansion [80]. At high temperatures and RP contents (> 40 °C, 1:2 P407:31R1), the large amount of hydrophobic material in the micelle core (PPO and small molecules) paired with the worsening PEO solubility causes the micelles to become destabilized, resulting in a complete loss of crystalline order (Fig. 8b). This loss of structure is associated with a nearly two-order-of-magnitude reduction in G' and G'' (Fig. 8a). A similar catastrophic reduction in modulus is observed in the drug-loaded formulations at lower 31R1 contents (Fig. S27). As in analogous system without small molecules, a small secondary peak in the DSC trace is observed at high temperatures. This secondary peak is more pronounced than in the formulations without small molecules and also corresponds to the temperatures at which the moduli begin decreasing. Based on the clouding observed in the analogous systems without small molecules (SI.13), macrophase separation likely occurs at these temperatures; the secondary peak is likely more pronounced due to the addition of hydrophobic CPEs that further destabilize the gel at these temperatures. This interpretation is in agreement with reports of syneresis, where

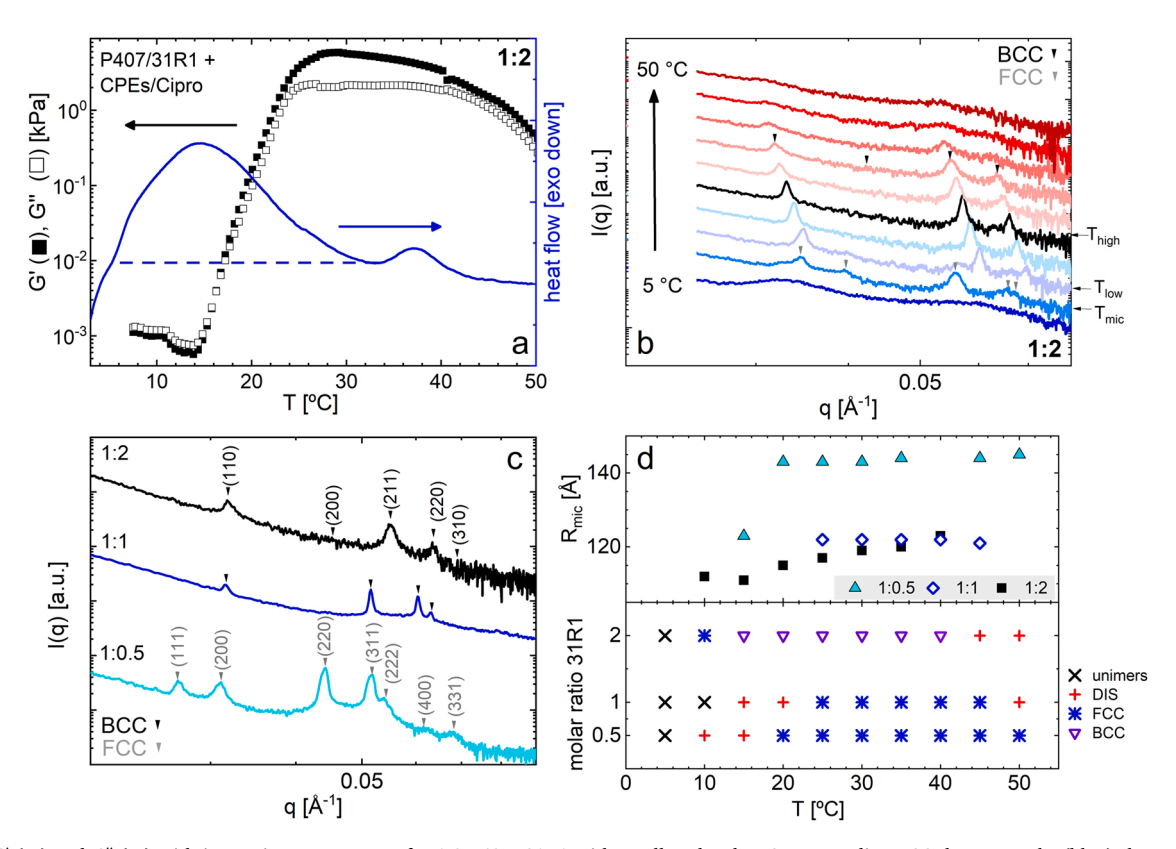


Fig. 8. (a)  $G'(\blacksquare)$  and  $G''(\square)$  with increasing temperature for 1:2 P407: 31R1 with small molecules. Corresponding DSC thermographs (blue) show a broad peak associated with co-micellization prior to gelation. (b) Corresponding 1D SAXS intensities every 5 °C from 5 °C to 50 °C show a transition from disordered micelles to FCC- to BCC-packed micelles with increasing T. At high T, BCC peaks disappear due to macrophase separation. (c) 1D SAXS intensities for drug-loaded 31R1-containing samples at 35 °C. (d) Summary of micelle  $R_t$  as a function of T and 31R1 content.

water or dilute solution is expelled from the concentrated gel, in P407 solutions in the presence of SDS (one of the CPEs) at elevated temperatures [69].

#### 4. Implications of small-molecule addition on hydrogel design

Small-molecule and RP additives give rise to differences in material properties that can impact clinical efficacy. In solutions with small molecules,  $T_{mic}$  is not linearly correlated with RP content for either 25R4 or 31R1 (Figs. 9a, SI.17). In the absence of small molecules, micellization is driven by worsening PPO-water interactions with increasing temperature [21-25]. RP addition increases the effective concentration and drives P407 to micellize at lower temperatures. Once small molecules are incorporated, unfavorable interactions between these compounds and water substantially contribute to micellization [81,105, 106]. As this process is more dependent upon small-molecule presence, T<sub>mic</sub> only slightly decreases between the 1:0.5 and 1:1 P407:RP formulations before plateauing. Similarly, the distance between the micellization and gelation transitions increases with 25R4 content in the absence of small molecules, yet this distance is uncorrelated with 25R4 content once small molecules are added (SI.16). These findings imply that the tunability of the micellization and gelation behavior via RP addition may be hindered by small-molecule addition; however, CPE content may provide an alternative route to tune these properties.

In comparison to formulations of pure P407 or P407 with RPs,  $\Delta H_{mic}$  is significantly reduced upon addition of small molecules, consistent with prior work [21,42]. Almgren and colleagues [107] reported that SDS binds primarily to the PPO midblock of poloxamers. Accordingly, DSC on formulations of 15% (w/v) P407 with each individual small molecule confirms that SDS is primarily responsible for this reduction in  $\Delta H_{mic}$  (Fig. S26). For systems containing 25R4, two distinct endothermic

dehydration steps occur [57,70,71]. The reported  $\Delta H_{mic}$  corresponds to the first step where P407 micellizes and 25R4 does not participate. While  $\Delta H_{mic}$  is two- to four-fold higher for 25R4 samples without small molecules vs. their drug-loaded counterparts, the difference in  $\Delta H_{b}$ , which corresponds to the dehydration of 25R4, between these formulations is much smaller (20 - 60% reduction upon small-molecule addition; Fig. 9c). Given that the majority of the small molecules are expected to incorporate into the micelle core during step one, the 25R4 bridging step should be relatively unaffected by small-molecule addition. Interestingly, small molecule addition reduces  $\Delta H_{mic}$  less drastically for 31R1-containing formulations (Fig. 9c). As 31R1 directly participates in the micellization process and the small-molecule content is constant, 31R1 addition dramatically increases the content of PPO relative to small molecules, such that SDS binding cannot as effectively reduce the enthalpic barrier to micellization.

Gelation occurs when the density of micelles is high enough to allow for strong inter-micelle interactions and overlap between coronas that drive the system to assemble into structures with long-range order. Small-molecule addition increases the micelle size as the CPEs/Cipro incorporate into the core. The resulting micelle volume fraction increases; thus,  $T_{gel}$  is lower for systems containing CPEs/Cipro relative to analogous systems without small molecules. This finding is potentially clinically useful, as  $T_{gel}$  in the 25R4-containing solutions without small molecules was too high to allow for effective gelation at physiological temperatures. Interestingly, while  $T_{gel}$  increased with increasing 25R4 content in the systems without small molecules, adding small molecules leads to a decrease in  $T_{gel}$  with both increasing 25R4 and 31R1 content. We attribute this difference to the micelle size; 25R4 "impurities" cannot as effectively block inter-micelle overlap when the overall micelle size is up to 50% larger because of small molecule addition.

Finally, consistent with the proposed mechanisms,  $G'_{max}$  is strongly

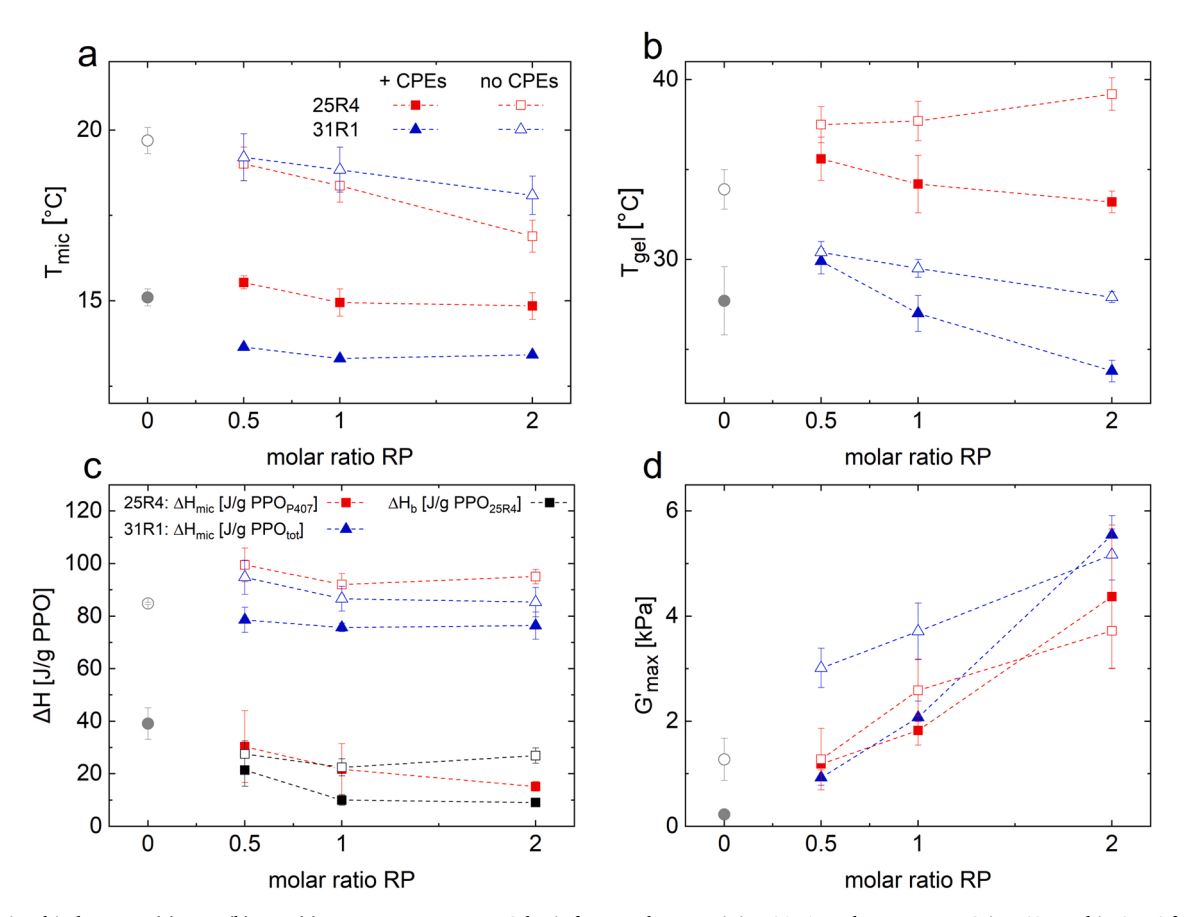


**Fig. 9.** Relationship between (a)  $T_{mic}$ , (b)  $T_{geb}$  (c)  $\Delta H$  on a per gram PPO basis for samples containing 31R1, and per gram PPO in P407 and in 25R4 for  $\Delta H_{mic}$  and  $\Delta H_{b}$ , respectively for the samples containing 25R4, (d) Max G' and molar ratio of RP for 25R4 and 31R1 with and without small molecules.

correlated with RP molar ratio in all systems (Fig. 9d). Small moleculecontaining formulations with RPs (1:0.5 and 1:1) exhibit a reduction in modulus similar to that observed when small molecules are added to P407; however, high RP-content formulations (1:2) containing small molecules appear to reverse this trend. While CPE addition typically leads to larger, weaker micelles, the higher moduli achieved in the 2:1 formulations with CPEs are likely due to the hypothesized changes in aggregation number and additional reinforcement provided by RP addition. Interestingly, despite very different incorporation mechanisms for the two RPs,  $G'_{max}$  is comparable for equivalent amounts of RP and small molecules. While bridging versus new micelle formation appears to impact  $G'_{max}$  in the absence of small molecules, this similarity in modulus suggests that once small molecules are added, the larger micelle size and/or total polymer content dictate(s) the maximum modulus, rather than the RP incorporation mechanism. Despite this similarity in  $G'_{max}$ , the samples containing 31R1 exhibit poor rheological stability at temperatures near physiological conditions due to clouding/ syneresis. This structural instability makes formulations with 31R1 less clinically applicable than those containing 25R4, which remain stable well above body temperature.

#### 5. Conclusions

This study investigated the thermoresponsive micellization and gelation of poloxamer P407 with incorporated small molecules and reverse poloxamers. The addition of reverse poloxamer 25R4 or 31R1 to P407 systems affects transition temperatures, rheological properties, and assembly. Further, the identity of the RP has a significant effect on the incorporation mechanism. For formulations containing 25R4, micellization and incorporation occur in a two-step process with increasing temperature, where P407 first micellizes and then 25R4 incorporates via bridging in step two. The addition of 25R4 results in the formation of a bridged, network-spanning gel with enhanced rheological properties (increased G') over the bare P407 system. While P407 solutions arrange into FCC-packed micelles upon heating, 25R4 addition causes the systems to arrange first into BCC-packed micelles and then to rearrange into FCC packing upon further heating. This difference is attributed to a change in the inter-micelle potential that is caused by the presence of RP and diblock impurities. As 31R1 has a much higher PPO fraction than 25R4, its mechanism for incorporation involves comicellization. In systems containing 31R1, micellization and RP incorporation occur in a single step, where 31R1 chains displace up to six P407 chains from each micelle core. Free P407 chains then form a greater number of micelles, driving gelation at lower temperatures.

As has been shown previously, the addition of hydrophobic small molecules to P407 weakens the gel and lowers the gelation temperature while expanding the size of the micelles packed in an FCC structure. Addition of either 25R4 and 31R1 enhances the rheological properties of these drug-loaded formulations, but it reduces the ability to tune the resulting thermal transitions via RP addition. However, varying the molar ratio of RP still allows for some flexibility in tuning the gelation temperature, rheological properties, and ordered structures. Further, variation in RP identity changes the underlying assembly mechanism and macromolecular structure. Addition of 25R4 leads to the formation of bridged structures with enhanced moduli that are stable upon smallmolecule incorporation. Previous work has shown that physical bridging across micelles does not hinder small-molecule diffusion when total polymer content is held constant. As such, 25R4 addition provides a promising avenue for enhancing the mechanical properties of the gels, potentially without sacrificing small-molecule diffusion necessary for therapeutic delivery. Understanding and controlling these selfassembled structures will facilitate the creation of antibiotic-loaded hydrogel systems with targeted gelation temperatures and mechanical properties to optimize diffusion and adhesion.

#### CRediT authorship contribution statement

**Michelle Calabrese:** Conceptualization, Supervision, Project administration, Writing – review & editing **Joanna White:** Methodology, Investigation, Formal analysis, Writing – original draft, Writing – review & editing

#### **Declaration of Competing Interest**

The authors declare that they have no known competing financial interests or personal relationships that could have appeared to influence the work reported in this paper.

#### Acknowledgements

This material is based upon work supported by the National Science Foundation Graduate Research Fellowship under Grant No. CON-75851, Project 00074041. Any opinions, findings, and conclusions or recommendations expressed in this material are those of the author(s) and do not necessarily reflect the views of the National Science Foundation. Research reported in this publication was supported by The National Institute on Deafness and Other Communication Disorders of the National Institutes of Health under award number R21DC019184-01A1. This research used resources of the Advanced Photon Source, a U.S. Department of Energy (DOE) Office of Science User Facility, operated for the DOE Office of Science by Argonne National Laboratory under Contract No. DE-AC02-06CH11357. SAXS experiments were carried out at Sector 5 of the Advanced Photon Source. The Sector 5 DuPont-Northwestern-Dow Collaborative Access Team (DND-CAT) was supported by E.I. DuPont de Nemours & Co., the Dow Chemical Company, and Northwestern University. Lab-source SAXS experiments were carried out at the Characterization Facility, University of Minnesota, which receives partial support from the NSF through the MRSEC (Award Number DMR-2011401) and the NNCI (Award Number ECCS-2025124) programs. The authors thank the Anton Paar VIP program for the rheometer used in this work. NMR instruments reported in this publication were supported by the Office of the Vice President of Research, College of Science and Engineering, and the Department of Chemistry at the University of Minnesota.

# Appendix A. Supporting information

Supplementary data associated with this article can be found in the online version at doi:10.1016/j.colsurfa.2021.128246.

# References

- S.D. Singh-Joy, V.C. McLain, Safety assessment of poloxamers 101, 105, 108, 122, 123, 124, 181, 182, 183, 184, 185, 188, 212, 215, 217, 231, 234, 235, 237, 238, 282, 284, 288, 331, 333, 334, 335, 338, 401, 402, 403, and 407, poloxamer 105 benzoate, and poloxamer 182 dibenzoate as used in cosmetics, Int. J. Toxicol. 27 (2008) 93
- [2] T. Bai, Y. Liu, J. Liu, C. Yu, W. Jiang, Y. Fan, A comparison of different surfactants on foam stability in foam sclerotherapy in vitro, J. Vasc. Surg. 69 (2019) 581.
- [3] J. Unosson, E.B. Montufar, H. Engqvist, M.P. Ginebra, C. Persson, Brushite foamsthe effect of Tween® 80 and Pluronic® F-127 on foam porosity and mechanical properties, J. Biomed. Mater. Res. B 104 (2016) 67.
- [4] M. Asama, A. Hall, Y. Qi, B. Moreau, H. Walthier, M. Schaschwary, B. Bristow, Q. Wang, Alternative foaming agents for topical treatment of ulcerative colitis, J. Biomed. Mater. Res. A 106 (2018) 1448.
- [5] D. Ćirin, V. Krstonošić, Influence of poloxamer 407 on surface properties of aqueous solutions of polysorbate surfactants, J. Surfactants Deterg. 23 (2020) 505
- [6] M.A. James-Smith, D. Shekhawat, S. Cheung, B.M. Moudgil, D.O. Shah, Role of ethylene oxide and propylene oxide groups of pluronics in binding of fatty acid to pluronics in microemulsions, J. Surfactants Deterg. 11 (2008) 237.
- [7] M. Fernandez-Tarrio, F. Yañez, K. Immesoete, C. Alvarez-Lorenzo, A. Concheiro, Pluronic and tetronic copolymers with polyglycolyzed oils as self-emulsifying drug delivery systems, AAPS PharmSciTech 9 (2008) 471.
- [8] A. Pitto-Barry, N.P. Barry, Pluronic® block-copolymers in medicine: from chemical and biological versatility to rationalisation and clinical advances Polym, Polym. Chem. 5 (2014) 3291.

- [9] C. Zhang, J. Zhang, Y. Qin, H. Song, P. Huang, W. Wang, C. Wang, C. Li, Y. Wang, D. Kong, Co-delivery of doxorubicin and pheophorbide A by pluronic F127 micelles for chemo-photodynamic combination therapy of melanoma, J. Mater. Chem. B 6 (2018) 3305.
- [10] A.R. Fares, A.N. ElMeshad, M.A.A. Kassem, Enhancement of dissolution and oral bioavailability of lacidipine via pluronic P123/F127 mixed polymeric micelles: formulation, optimization using central composite design and in vivo bioavailability study, Drug Deliv. 25 (2018) 132.
- [11] X. Wu, W. Ge, T. Shao, W. Wu, J. Hou, L. Cui, J. Wang, Z. Zhang, Enhancing the oral bioavailability of biochanin A by encapsulation in mixed micelles containing Pluronic F127 and Plasdone S630, Int. J. Nanomed. 12 (2017) 1475.
- [12] H. Abdeltawab, D. Svirskis, B.J. Boyd, A. Hill, M. Sharma, Injectable thermoresponsive gels offer sustained dual release of bupivacaine hydrochloride and ketorolac tromethamine for up to two weeks, Int. J. Pharm. 604 (2021).
- [13] V.P. Torchilin, Structure and design of polymeric surfactant-based drug delivery systems, J. Control. Release 73 (2001) 137.
- [14] L.L. Tundisi, R. Yang, L.P.P. Borelli, T. Alves, M. Mehta, M.V. Chaud, P. G. Mazzola, D.S. Kohane, Enhancement of the mechanical and drug-releasing properties of poloxamer 407 hydrogels with casein, Pharm. Res. 38 (2021) 515.
- [15] L. Djekic, B. Čalija, Medarević, Gelation behavior, drug solubilization capacity and release kinetics of poloxamer 407 aqueous solutions: The combined effect of copolymer, cosolvent and hydrophobic drug, J. Mol. Liq. 303 (2020), 112639.
- [16] G. Dumortier, J.L. Grossiord, F. Agnely, J.C. Chaumeil, Expert review a review of poloxamer 407 pharmaceutical and pharmacological characteristics, Pharm. Res. 23 (2006) 2709.
- [17] D. Jain, V. Kumar, S. Singh, A. Mullertz, D. Bar-Shalom, Newer trends in in situ gelling systems for controlled ocular drug delivery, J. Anal. Pharm. Res. 2 (2016).
- [18] E.J. Ricci, M.V. Bentley, M. Farah, R.E. Bretas, J.M. Marchetti, Rheological characterization of Poloxamer 407 lidocaine hydrochloride gels, Eur. J. Pharm. Sci. 17 (2002) 161.
- [19] Inactive Ingredient Search for Approved Drug Products, U.S. Food Drug Administration. (https://www.accessdata.fda.gov/scripts/cder/iig/index.cfm).
- [20] G.S. Kwon, K. Kataoka, Block copolymer micelles as long-circulating drug vehicles, Adv. Drug Deliv. Rev. 16 (1995) 295.
- [21] R. Basak, R. Bandyopadhyay, Encapsulation of hydrophobic drugs in Pluronic F127 micelles: effects of drug hydrophobicity, solution temperature, and pH, Langmuir 29 (2013) 4350.
- [22] E. Ruel-Gariépy, J.-C. Leroux, In situ-forming hydrogels-review of temperaturesensitive systems, Eur. J. Pharm. Biopharm. 58 (2004) 409.
- [23] K. Mortensen, W. Brown, Poly(ethylene oxide)-poly(propylene oxide)-poly (ethylene oxide) triblock copolymers in aqueous solution. The influence of relative block size, Macromolecules 26 (1993) 4128.
- [24] G. Wanka, H. Hoffmann, W. Ulbricht, Phase diagrams and aggregation behavior of poly(oxyethylene)-poly(oxypropylene)-poly(oxyethylene) triblock copolymers in aqueous solutions. Macromolecules 27 (1994) 4145.
- [25] P. Parekh, J. Dey, S. Kumar, S. Nath, R. Ganguly, V. Aswal, P. Bahadur, Butanol solubilization in aqueous F127 solution: investigating the enhanced micellar solvation and consequent improvement in gelation characteristics, Colloids Surf. B Biointerfaces 114 (2014) 386.
- [26] P. Alexandridis, J.F. Holzwarth, T.A. Hatton, Micellization of poly (ethylene oxide)-poly (propylene oxide)-poly (ethylene oxide) triblock copolymers in aqueous solutions: thermodynamics of copolymer association, Macromolecules 27 (1994) 2414
- [27] P. Bahadur, K. Pandya, M. Almgren, P. Li, P. Stilbs, Effect of inorganic salts on the micellar behaviour of ethylene oxide-propylene oxide block copolymers in aqueous solution, Colloid Polym. Sci. 271 (1993) 657.
- [28] P. McCauley, S. Kumar, M. Calabrese, Criteria governing rod formation and growth in nonionic polymer wormlike micelles, Langmuir 37 (2021) 11676–11687.
- [29] E.Y. XiLoh, M.B. Fauzi, M.H. Ng, P.Y. Ng, S.F. Ng, H. Ariffin, M.C.I. MohdAmin, Cellular and molecular interaction of human dermal fibroblasts with bacterial nanocellulose composite hydrogel for tissue regeneration, ACS Appl. Mater. Interfaces 10 (2018) 39532.
- [30] E. Russo, C. Villa, Poloxamer hydrogels for biomedical applications, Pharmaceutics 11 (2019).
- [31] N.P. Murphy, K.J. Lampe, Mimicking biological phenomena in hydrogel-based biomaterials to promote dynamic cellular responses, J. Mater. Chem. 3 (2015) 7867
- [32] J. Wang, R. Youngblood, L. Cassinotti, M. Skoumal, G. Corfas, L. Shea, An injectable PEG hydrogel controlling neurotrophin-3 release by affinity peptides, J. Control. Release 330 (2021) 575.
- [33] F. Cao, X. Zhang, Q. Ping, Drug Delivery New method for ophthalmic delivery of azithromycin by poloxamer/carbopol-based in situ gelling system, Drug Deliv. 17 (2010) 500.
- [34] W. Wang, E. Wat, P.C.L. Hui, B. Chan, F.S.F. Ng, C.-W. Kan, X. Wang, H. Hu, E.C. W. Wong, C.B.S. Lau, P.-C. Leung, Dual-functional transdermal drug delivery system with controllable drug loading based on thermosensitive poloxamer hydrogel for atopic dermatitis treatment, Sci. Rep. 6 (2016) 1.
- [35] E. Giuliano, D. Paolino, M. Fresta, D. Cosco, Mucosal applications of poloxamer 407-based hydrogels: an overview, Pharmaceutics 10 (2018).
- [36] L. Ci, Z. Huang, Y. Liu, Z. Liu, G. Wei, W. Lu, Amino-functionalized poloxamer 407 with both mucoadhesive and thermosensitive properties: preparation, characterization and application in a vaginal drug delivery system, Acta Pharm. Sin. B 7 (2017) 593.
- [37] A.C. Akkari, J.Z. Papini, G.K. Garcia, M.K. Franco, L.P. Cavalcanti, A. Gasperini, M.I. Alkschbirs, F. Yokaichyia, E. De Paula, G.R. Tófoli, D.R. De Araujo,

- Poloxamer 407/188 binary thermosensitive hydrogels as delivery systems for infiltrative local anesthesia: physico-chemical characterization and pharmacological evaluation, Mater. Sci. Eng. C 68 (2016) 299.
- [38] A.L. Edmunds, Otiprio: an FDA-approved ciprofloxacin suspension gel for pediatric otitis media with effusion, Pharmacol. Ther 42 (2017) 307.
- [39] M.A. Grimaudo, S. Pescina, C. Padula, P. Santi, A. Concheiro, C. Alvarez-Lorenzo, S. Nicoli, Poloxamer 407/TPGS mixed micelles as promising carriers for cyclosporine ocular delivery, Mol. Pharm. 15 (2018) 571.
- [40] I.S. Kurniawansyah, T. Rusdiana, I. Sopyan, H. Ramoko, H.A. Wahab, A. Subarnas, In situ ophthalmic gel forming systems of poloxamer 407 and hydroxypropyl methyl cellulose mixtures for sustained ocular delivery of chloramphenicole: optimization study by factorial design, Heliyon 6 (2020), e05365
- [41] K.V. Tobin, J. Fiegel, N.K. Brogden, Thermosensitive gels used to improve microneedle-assisted transdermal delivery of naltrexone, Polymers 13 (2021).
- [42] R. Yang, V. Sabharwal, O.S. Okonkwo, N. Shlykova, R. Tong, L.Y. Lin, W. Wang, S. Guo, J.J. Rosowski, S.I. Pelton, D.S. Kohane, Treatment of otitis media by transtympanic delivery of antibiotics, Sci. Transl. Med. 8 (2016), 356ra120.
- [43] R. Yang, V. Sabharwal, N. Shlykova, O.S. Okonkwo, S.I. Pelton, D.S. Kohane, Treatment of Streptococcus pneumoniae otitis media in a chinchilla model by transtympanic delivery of antibiotics, JCI Insight 3 (2018) 1.
- [44] R. Yang, O.S. Okonkwo, D. Zurakowski, D.S. Kohane, Synergy between chemical permeation enhancers and drug permeation across the tympanic membrane, J. Control. Release 289 (2018) 94.
- [45] C.S. Yong, J.S. Choi, Q.Z. Quan, J.D. Rhee, C.K. Kim, S.J. Lim, K.M. Kim, P.S. Oh, H.G. Choi, Effect of sodium chloride on the gelation temperature, gel strength and bioadhesive force of poloxamer gels containing diclofenac sodium, Int. J. Pharm. 226 (2001) 195.
- [46] R.B. Walker, E.W. Smith, The role of percutaneous penetration enhancers, Adv. Drug Deliv. Rev. 18 (1996) 295.
- [47] M. Levy, M. Y. Wang, J. K. Armstrong, T. C. Fisher, Bone hemostasis method and materials, US Patent No. 9,616,150 (2017).
- [48] V. Nace, Nonionic Surfactants: Polyoxyalkylene Block Copolymers 60, CRC Press, 1996, pp. 220–253.
- [49] T. Kojarunchitt, S. Baldursdottir, Y.-D. Dong, B.J. Boyd, T. Rades, S. Hook, Modified thermoresponsive Poloxamer 407 and chitosan sol-gels as potential sustained-release vaccine delivery systems, Eur. J. Pharm. Biopharm. 89 (2015) 74
- [50] Y. Xie, J. Tang, Z. Lu, Z. Sun, L. An, Effects of poly(propylene oxide)-poly (ethylene oxide)-poly(propylene oxide) triblock copolymer on the gelation of poly(ethylene oxide)-poly(propylene oxide)-poly(ethylene oxide) aqueous solutions, J. Macromol. Sci. 52 (2013) 1183.
- [51] B.Z. Chowdhry, M.J. Snowden, S.A. Leharne, A scanning calorimetric investigation of phase transitions in a PPO-PEO-PPO block copolymer, Eur. Polym. J. 35 (1999) 273.
- [52] G. D'Errico, L. Paduano, A. Khan, Temperature and concentration effects on supramolecular aggregation and phase behavior for poly(propylene oxide)-b-poly (ethylene oxide)- b-poly(propylene oxide) copolymers of different composition in aqueous mixtures, J. Colloid Interface Sci. 279 (2004) 379.
- [53] G. D'Errico, L. Paduano, O. Ortona, G. Mangiapia, L. Coppola, F.L. Celso, Temperature and concentration effects on supramolecular aggregation and phase behavior for poly(propylene oxide)-b-poly(ethylene oxide)-b-poly(propylene oxide) copolymers of different concentration in aqueous mixtures, 2, J. Colloid Interface Sci. 359 (2011) 179.
- [54] B. Naskar, S. Ghosh, S.P. Moulik, Solution behavior of normal and reverse triblock copolymers (Pluronic L44 and 10R5) individually and in binary mixture, Langmuir 28 (2012) 7134.
- [55] E. Larrañeta, J.R. Isasi, Phase behavior of reverse poloxamers and poloxamines in water, Langmuir 29 (2013) 1045.
- [56] Q. Wang, L. Li, S. Jiang, Effects of a PPO-PEO-PPO triblock copolymer on micellization and gelation of a PEO-PPO-PEO triblock copolymer in aqueous solution, Langmuir 21 (2005) 9068.
- [57] S. Liu, L. Li, Molecular interactions between PEO-PPO-PEO and PPO-PEO-PPO triblock copolymers in aqueous solution, Colloids Surf. A Physicochem. Eng. Asp. 484 (2015) 485.
- [58] O. Ortona, G. D'Errico, L. Paduano, V. Vitagliano, Interaction between cationic, anionic, annd non-ionic surfactants with ABA block copolymer Pluronic PE6200 and with BAB reverse block copolymer Pluronic 25R4, J. Colloid Interface Sci. 301 (2006) 63.
- [59] S. Liu, H. Bao, L. Li, Role of PPO-PEO-PPO triblock copolymers in phase transitions of a PEO-PPO-PEO triblock copolymer in aqueous solution, Eur. Polym. J. 71 (2015) 423.
- [60] L.A. Rankin, B. Lee, K.P. Mineart, Effect of network connectivity on the mechanical and transport properties of block copolymer gels, J. Polym. Sci. 59 (2021) 34.
- [61] T. Kojarunchitt, S. Hook, S. Rizwan, T. Rades, S. Baldursdottir, Development and characterisation of modified poloxamer 407 thermoresponsive depot systems containing cubosomes, Int. J. Pharm. 408 (2011) 20.
- [62] A.M. Bodratti, P. Alexandridis, Functional biomaterials formulation of poloxamers for drug delivery, J. Funct. Biomater. 9 (2018).
- [63] W. Boonlai, V. Tantishaiyakul, N. Hirun, T. Sangfai, K. Suknuntha, Thermosensitive poloxamer 407/poly(acrylic acid) hydrogels with potential application as injectable drug delivery system, AAPS PharmSciTech 19 (2018) 2103.

- [64] N. Hirun, V. Tantishaiyakul, T. Sangfai, W. Boonlai, S. Soontaranon, S. Rugmai, The effect of poly(acrylic acid) on temperature-dependent behaviors and structural evolution of poloxamer, Polym. Int. 70 (2021) 1282–1289.
- [65] C. Ju, J. Sun, P. Zi, X. Jin, C. Zhang, Thermosensitive micelles-hydrogel hybrid system based on poloxamer 407 for localized delivery of paclitaxel, J. Pharm. Sci. 102 (2013) 2707.
- [66] P.C. Sharma, A. Jain, S. Jain, R. Pahwa, Mohammad, S. Yar, Ciprofloxacin: review on developments in synthetic, analytical, and medicinal aspects, J. Enzyme Inhib. Med. Chem 25 (2010) 577.
- [67] F. Varanda, M.J. Pratas De Melo, A.I. Caço, R. Dohrn, F.A. Makrydaki, E. Voutsas, D. Tassios, I.M. Marrucho, Solubility of Antibiotics in Different Solvents. 1. Hydrochloride Forms of Tetracycline, Moxifloxacin, and Ciprofloxacin, Ind. Eng. Chem. Res. 45 (2006) 6368.
- [68] I. Dal, O. Pereira, F.R. Cunha, Rheological response in shear flows of a thermosensitive elastic liquid in the presence of some additives, Rheol. Acta 59 (2020) 307
- [69] E. Hecht, K. Mortensen, M. Gradzielski, H. Hoffmann, Interaction of ABA block copolymers with ionic surfactants: influence on micellization and gelation, J. Phys. Chem. 99 (1995) 4866.
- [70] L. Li, L.H. Lim, Q. Wang, S.P. Jiang, Thermoreversible micellization and gelation of a blend of pluronic polymers, Polymer 49 (1952) (2008).
- [71] H. Ren, X.-P. Qiu, Y. Shi, P. Yang, F.M. Winnik, The two phase transitions of hydrophobically end-capped poly(n-isopropylacrylamide)s in water, Macromolecules 53 (2020) 5105.
- [72] P.A. Heiney, Datasqueeze: A software tool for powder and small-angle x-ray diffraction analysis, IUCr Newsletter 32 (2005) 9.
- [73] I. Akiba, N. Terada, S. Hashida, K. Sakurai, T. Sato, K. Shiraishi, M. Yokoyama, H. Masunaga, H. Ogawa, K. Ito, N. Yagi, Encapsulation of a hydrophobic drug into a polymer-micelle core explored with synchrotron SAXS, Langmuir 26 (2010) 7544
- [74] A. Bogomolova, M. Hruby, J. Panek, M. Rabyk, S. Turner, S. Bals, M. Steinhart, A. Zhigunov, O. Sedlacek, P. Stepanek, S. Filippov, Small-angle X-ray scattering and light scattering study of hybrid nanoparticles composed of thermoresponsive triblock copolymer F127 and thermoresponsive statistical polyoxazolines with hydrophobic moieties, J. Appl. Crystallogr. 46 (1690) (2013).
- [75] R.K. Prud'homme, G. Wu, D.K. Schneider, Structure and rheology studies of poly (oxyethylene- oxypropylene- oxyethylene) aqueous solution, Langmuir 12 (1996) 4651
- [76] L. Guo, R.H. Colby, M.Y. Lin, G.P. Dado, Micellar structure changes in aqueous mixtures of nonionic surfactants. J. Rheol. 45 (2001) 1223.
- [77] I.W. Hamley, V. Castelletto, Small-angle scattering of block copolymers: in the melt, solution and crystal states, Prog. Polym. Sci. 29 (2004) 909.
- [78] F. Artzner, S. Geiger, A. Olivier, C. Allais, S. Finet, F. Agnely, Interactions between poloxamers in aqueous solutions: micellization and gelation studied by differential scanning calorimetry, small angle x-ray scattering, and rheology, Langmuir 23 (2007) 5085.
- [79] E. Kushan, E. Senses, Thermoresponsive and injectable composite hydrogels of cellulose nanocrystals and pluronic F127, ACS Appl. Bio Mater 4 (2021) 3507.
- [80] K. Mortensen, W. Batsberg, S. Hvidt, Effects of PEO-PPO Diblock Impurities on the cubic structure of aqueous PEO-PPO-PEO pluronics micelles: FCC and BCC ordered structures in F127, Macromolecules 41 (1720) (2008).
- [81] C.-F. Lee, M.-R. Wang, T.-L. Lin, C.-H. Yang, L.-J. Chen, Dynamic behavior of the structural phase transition of hydrogel formation induced by temperature ramp and addition of ibuprofen, Langmuir 36 (2020) 8929.
- [82] M.T. Cook, P. Haddow, S.B. Kirton, W.J. McAuley, Polymers exhibiting lower critical solution temperatures as a route to thermoreversible gelators for healthcare, Adv. Funct. Mater. 31 (2021), 2008123.
- [83] M. Bohorquez, C. Koch, T. Trygstad, N. Pandit, A study of the temperaturedependent micellization of pluronic F127, J. Colloid Interface Sci. 216 (1999) 34.
- [84] B. Shriky, A. Kelly, M. Isreb, M. Babenko, N. Mahmoudi, S. Rogers, O. Shebanova, T. Snow, T. Gough, Pluronic F127 thermosensitive injectable smart hydrogels for controlled drug delivery system development, J. Colloid Interface Sci. 565 (2020) 119.
- [85] H.J. Park, G.M. Treich, Z.D. Helming, J.E. Morgan, C.Y. Ryu, H.S. Hwang, G. Y. Jung, Micellar packing of pluronic block copolymer solutions: polymeric impurity effects, Macromol. Res. 23 (2015) 13.
- [86] K. Suman, S. Sourav, Y.M. Joshi, Rheological signatures of gel-glass transition and a revised phase diagram of an aqueous triblock copolymer solution of Pluronic F127, Phys. Fluids 33 (2021), 073610.

- [87] P. Parekh, J. Dey, S. Kumar, S. Nath, R. Ganguly, V. Aswal, P. Bahadur, Butanol solubilization in aqueous f127 solution: Investigating the enhanced micellar solvation and consequent improvement in gelation characteristics, Colloids and Surfaces B Biointerfaces 114 (2014) 386.
- [88] N.A.K. Meznarich, K.A. Juggernauth, K.M. Batzli, B.J. Love, Structural changes in PEO-PPO-PEO gels induced by methylparaben and dexamethasone observed using time-resolved SAXS, Macromolecules 44 (2011) 7792.
- [89] G. Wanka, H. Hoffmann, W. Ulbricht, The aggregation behavior of poly-(oxyethylene)-poly-(oxypropylene)-poly-(oxyethylene)-block-copolymers in aqueous solution, Colloid Polym. Sci. 268 (1990) 101.
- [90] G. Pérez-Sánchez, F.A. Vicente, N. Schaeffer, I.S. Cardoso, S.P. Ventura, M. Jorge, J. Coutinho, Rationalizing the phase behavior of triblock copolymers through experiments and molecular simulations, J. Phys. Chem. C 123 (2019) 21224.
- [91] P. Alexandridis, J.F. Holzwarth, Differential scanning calorimetry investigation of the effect of salts on aqueous solution properties of an amphiphilic block copolymer (poloxamer), Langmuir 13 (1997) 6074.
- [92] G.A. McConnell, A.P. Gast, J.S. Huang, S.D. Smith, Disorder-order transitions in soft sphere polymer micelles, Phys. Rev. Lett. 71 (1993) 2102.
- [93] T.P. Lodge, J. Bang, M.J. Park, K. Char, Origin of the thermoreversible fcc-bcc transition in block copolymer solutions, Phys. Rev. Lett. 92 (2004), 145501.
- [94] I.W. Hamley, J.A. Pople, O. Diat, A thermally induced transition from a bodycentered to a face-centered cubic lattice in a diblock copolymer gel, Colloid Polym. Sci. 276 (1998) 446.
- [95] T. Liu, B. Chu, Formation of homogeneous gel-like phases by mixed triblock copolymer micelles in aqueous solution: FCC to BCC phase transition, J. Appl. Cryst. 33 (2000) 727.
- [96] C.M. de Lima, S.M.C. Siqueira, A.F.V. de Amorim, K.B.S. Costa, D.H.A. de Brito, M.E.N.P. Ribeiro, N.M.P.S. Ricardo, C. Chaibunditc, S.G. Yeates, N.M.P. S. Ricardo, Effects of polypropylene glycol 400 (PPG400) on the micellization and gelation of pluronic F127, Macromolecules 48 (2015) 7978.
- [97] Y.H. Hsu, H.W. Tsui, S.Y. Lin, L.J. Chen, The origin of anomalous positive heat capacity change upon micellization of Pluronic triblock copolymer F108 in aqueous solutions: effect of PEO-PPO diblock impurities, Colloids Surf. A Physicochem. Eng. Asp 509 (2016) 109.
- [98] J.C. Shah, M. Maniar, pH-dependent solubility and dissolution of bupivacaine and its relevance to the formulation of a controlled release system, J. Control. Release 23 (1993) 261.
- [99] Y. Zhu, W. Xu, J. Zhang, Y. Liao, C.K. Firempong, M. Adu-Frimpong, W. Deng, H. Zhang, J. Yu, X. Xu, Self-microemulsifying drug delivery system for improved oral delivery of limonene: preparation, characterization, in vitro and in vivo evaluation, AAPS PharmSciTech 20 (2019).
- [100] H.A. Massaldi, C.J. King, Simple technique to determine solubilities of sparingly soluble organics: solubility and activity coefficients of d-Limonene, n-Butylbenzene, and n-Hexyl acetate in water and sucrose solutions, J. Chem. Eng. Data 18 (1973) 393.
- [101] A.M. Khan, S.S. Shah, pH induced partitioning and interactions of ciprofloxacin hydrochloride with anionic surfactant sodium dodecyl sulfate using ultraviolet and fourier transformed infrared spectroscopy study, J. Dispers. Sci. Technol. 30 (2009) 1247.
- [102] A.M. Khan, S.S. Shah, Fluorescence spectra behavior of ciprofloxacin HCl in aqueous medium and its interaction with sodium dodecyl sulfate, J. Dispers. Sci. Technol. 30 (2009) 997.
- [103] D. Wei, L. Ge, R. Guo, Effect of hydrophilically modified ibuprofen on thermoresponsive gelation of pluronic copolymer, Colloids Surf. A Physicochem. Eng. Asp 553 (2018) 1.
- [104] A.L. Thompson, L.M. Mensah, B.J. Love, The effect of cisplatin on the nanoscale structure of aqueous PEO-PPO-PEO micelles of varying hydrophilicity observed using SAXS, Soft Matter 15 (2019) 3970.
- [105] S. Kancharla, N.A. Zoyhofski, L. Bufalini, B.F. Chatelais, P. Alexandridis, Association between nonionic amphiphilic polymer and ionic surfactant in aqueous solutions: effect of polymer hydrophobicity and micellization, Polymers 12 (2020)
- [106] R. Ganguly, V.K. Aswal, P.A. Hassan, I.K. Gopalakrishnan, S.K. Kulshreshtha, Effect of SDS on the self-assembly behavior of the PEO-PPO-PEO triblock copolymer (EO) 20 (PO) 70 (EO) 20, J. Phys. Chem. B 20 (2006) 9843.
- [107] M. Almgren, J. Van Stem, C. Lindblad, P. Li, P. Stilbs, P. Bahadur, Aggregation of poly(ethylene oxlde)-poly(propylene oxlde)-poly(ethylene oxide) triblock copolymers in the presence of sodium dodecyl sulfate in aqueous solution, J. Phys. Chem. 95 (1991) 5677.